



**POLITECNICO**  
MILANO 1863

SCUOLA DI INGEGNERIA INDUSTRIALE  
E DELL'INFORMAZIONE

# Numerical Modelling of single impacts during Ultrasonic shot peening

TESI DI LAUREA MAGISTRALE IN  
MECHANICAL ENGINEERING  
INGEGNERIA MECCANICA

**Author: Aravind Swaminathan**

Student ID: 10815143

Advisor: Prof. Mario Guagliano

Co-advisor: Prof. Sara Bagherifard  
Erencan Oranli

Academic Year: 2023-24



## Acknowledgments

I would firstly like to thank Prof. Mario GUAGLIANO for his precious leading and guidance. Every one of my meetings with him has been a source of inspiration for me and kept me motivated to learn and work more than the previous day.

I would like to thank Prof. Sara BAGHERIFARD for her continuous support over the entire study. It has been with her effort that the study kept on track and be successful. I am grateful to Erencan ORANLI for his valuable contribution to my Finite Elements Analysis numerical model. His help is what made the model accomplish its task.

I would like to thank my family and friends for their support. Their faith on me over the years is what characterizes this thesis.



## Abstract

Ultrasonic shot peening is a type of peening operation which is used to plastically deform the surface of the target material with high severity in order to produce desired material, surface and microstructural characteristics like a compressive residual stress layer and refined grain structure zone in that material. This is made possible by the usage of shots that impinges the target material with high frequency. For the concept of this thesis, a numerical model of a single shot impacting the target surface is created. Model considers material parameters and process parameters of ultrasonic shot peening. The model takes into account the variation of impact orientation and corresponding variation in impact velocity of the shots and delivers the change in the indentation geometry and restitution coefficient as outcomes under impacts with different orientations. The model stands as a solid reference for future work where multiple impact analysis could be investigated for the complete modeling of the treatment.

**Keywords:** Ultrasonic shot peening, Surface treatment, Finite element analysis, Numerical model.



## Sommario

La pallinatura ultrasonica è un tipo di operazione di pallinatura che viene utilizzata per deformare plasticamente la superficie del materiale target con elevata severità al fine di produrre le caratteristiche desiderate di materiale, superficie e microstruttura come uno strato di stress residuo compressivo e una zona di struttura granulare raffinata in quel materiale. Ciò è reso possibile dall'uso di colpi che colpiscono il materiale target con alta frequenza. Per il concetto di questa tesi, viene creato un modello numerico di un singolo colpo che impatta sulla superficie target. Il modello considera i parametri del materiale e i parametri di processo della pallinatura ultrasonica. Il modello tiene conto della variazione dell'orientamento dell'impatto e della corrispondente variazione della velocità di impatto dei colpi e fornisce la modifica della geometria di indentazione e del coefficiente di restituzione come risultati sotto impatti con orientamenti diversi. Il modello rappresenta un solido riferimento per lavori futuri in cui l'analisi di impatti multipli potrebbe essere studiata per la modellazione completa del trattamento.

**Parole chiave:** Pallinatura ultrasonica, Trattamento superficiale, Analisi degli elementi finiti, Modello numerico.

# Contents

<b>Abstract .....</b>	<b>IV</b>
<b>Abstract in italiano.....</b>	<b>VI</b>
<b>Contents .....</b>	<b>VII</b>
<b>1 Introduction .....</b>	<b>1</b>
1.1. Shot Peening .....	2
1.2. Principles of Shot Peening .....	3
1.3. Applications of Shot Peening .....	4
1.4. Ultrasonic Shot Peening.....	6
1.5. Peening Parameters .....	8
1.6. Principles of Ultrasonic Shot Peening.....	15
1.7. Attributes of Ultrasonic Shot Peening .....	16
1.8. Comparisons between CSP and USP.....	17
1.9. Literature Review on Numerical Model of USP.....	18
1.10. Challenges and Solutions.....	26
<b>2 Numerical model build-up .....</b>	<b>27</b>
2.1. FEA Model for USP .....	27
2.2. Simulation Characterization.....	33
2.2.1. Target material characterization .....	33
2.2.2. Shot material characterization.....	35
2.2.3. Validation of material model.....	36
2.2.4. Shot velocity and orientation characterization .....	37
2.2.4.1 Relationship between 2D Velocity and Angle of impact .....	38
2.2.5. Step time characterization.....	39
2.2.6. Post Processing .....	42
<b>3 Results and Discussions .....</b>	<b>43</b>
3.1. Results for Simulations of Case 1 .....	43
3.1.1. Simulation 1 .....	44
3.1.2. Simulation 2 .....	46
3.1.3. Simulation 3 .....	48
3.1.4. Simulation 4 .....	50
3.1.5. Simulation 5 .....	52
3.1.6. Simulation 6 .....	54

3.2.	Results for Simulations of Case 2 .....	56
3.2.1.	Simulation 1 .....	57
3.2.2.	Simulation 2 .....	59
3.2.3.	Simulation 3 .....	61
3.2.4.	Simulation 4 .....	63
3.2.5.	Simulation 5 .....	65
3.2.6.	Simulation 6 .....	67
3.3.	Discussion on Results .....	69
3.3.1.	Dimple Characteristics .....	69
3.3.2.	Variation of COR.....	72
<b>4</b>	<b>Conclusions.....</b>	<b>75</b>
	<b>Bibliography.....</b>	<b>77</b>
<b>A</b>	<b>Appendix .....</b>	<b>83</b>

# List of Figures

Figure 1.1: Process visualization of shot peening process.....	2
Figure 1.2: Principle behind shot peening.....	3
Figure 1.3: Residual Stress post Surface Grinding in 4340 Steel (Hrc50) .....	5
Figure 1.4: A general depiction of USP Process .....	7
Figure 1.5: Peening Parameter vs Roughness.....	10
Figure 1.6: Peening time vs roughness .....	10
Figure 1.7: Coverage in terms of number of shots per unit area.....	12
Figure 1.8: Variation of the RS gradient as the coverage changes .....	12
Figure 1.9: Variation of the PEEQ gradient as the coverage changes.....	13
Figure 1.10: USP Principle.....	15
Figure 1.11: Attributes of Shot peening over grain reformation.....	20
Figure 1.12 Schematics of a dimple.....	24
Figure 1.13: Indent depth and Surface roughness vs Peening time (Alloy).....	25
Figure 2.1: Target (a) and shot Model (b).....	27
Figure 2.2: Generic representation of Assembly Module.....	30
Figure 2.3: A generic representation of Accoustic elements in Mesh Module.....	31
Figure 2.4: A generic representation of meshing Module .....	32
Figure 2.5 Equipments for experimental analysis.....	37
Figure 2.6: Depiction of 2D Velocity Vector.....	38
Figure 2.7: Graphical Representation for determining COR in the normal direction to the substrate surface .....	39
Figure 2.8: A graphical representation of measuring distance between the nodes.....	41
Figure 2.9: A generic representation of path created to plot dimple diameter and dimple height.....	42
Figure 3.1: Velocities along different directions.....	44
Figure 3.2: Dimple characteristics at 90-degree impact angle.....	44
Figure 3.3: Velocities along different directions.....	46
Figure 3.4: Dimple characteristics at 75-degree impact angle.....	46
Figure 3.5: Velocities along different directions.....	48

Figure 3.6: Dimple characteristics at 60-degree impact angle .....	48
Figure 3.7: Velocities along different directions.....	50
Figure 3.8: Dimple characteristics at 45-degree impact angle .....	50
Figure 3.9: Velocities along different directions.....	52
Figure 3.10: Dimple characteristics at 30-degree impact angle .....	52
Figure 3.11: Velocities along different directions.....	54
Figure 3.12: Dimple characteristics at 15-degree impact angle.....	54
Figure 3.13: Velocities along different directions.....	57
Figure 3.14: Dimple characteristics at 90-degree impact angle .....	57
Figure 3.15: Velocities along different directions.....	59
Figure 3.16: Dimple characteristics at 75-degree impact angle.....	59
Figure 3.17: Velocities along different directions.....	61
Figure 3.18: Dimple characteristics at 60-degree impact angle .....	61
Figure 3.19: Velocities along different directions.....	63
Figure 3.20: Dimple characteristics at 45-degree impact angle .....	63
Figure 3.21: Velocities along different directions.....	65
Figure 3.22: Dimple characteristics at 30-degree impact angle .....	65
Figure 3.23: Velocities along different directions.....	67
Figure 3.24: Dimple characteristics at 15-degree impact angle .....	67
Figure 3.25: Dimple morphology owing to different simulations under case 1 .....	70
Figure 3.26: Dimple morphology owing to different simulations under case 2.....	71
Figure 3.27: Variation of COR under case 1 .....	73
Figure 3.28: Variation of COR under case 2.....	74

# List of Tables

Table 1.1: Comparison of pneumatic CSP and USP. .... 17

Table 2.1: Density and Elastic Properties of the target material..... 34

Table 2.2: Parameters of Johnson-Cook Model..... 34

Table 2.3: Density and Elastic Properties of the Shot material ..... 35

Table 2.4: Validation of material model.....36

Table 3.1: variation in impact velocities wrt impact orientation with constant normal velocity.....43

Table 3.2: Dimple characteristics.....44

Table 3.3: COR along x direction. ....45

Table 3.4: COR along y direction.....45

Table 3.5: COR wrt 2D Velocity .....45

Table 3.6: Dimple characteristics.....46

Table 3.7: COR along x direction. ....47

Table 3.8: COR along y direction..... 47

Table 3.9: COR wrt 2D Velocity. ....47

Table 3.10: Dimple characteristics.....48

Table 3.11: COR along x direction. ....49

Table 3.12: COR along y direction.....49

Table 3.13: COR wrt 2D Velocity. ....49

Table 3.14: Dimple characteristics.....50

Table 3.15: COR along x direction. ....51

Table 3.16: COR along y direction.....51

Table 3.17: COR wrt 2D Velocity. ....51

Table 3.18: Dimple characteristics.....52

Table 3.19: COR along x direction. ....53

Table 3.20: COR along y direction.....53

Table 3.21: COR wrt 2D Velocity. ....53

Table 3.22: Dimple characteristics.....54

Table 3.23: COR along x direction. ....	55
Table 3.24: COR along y direction.....	55
Table 3.25: COR wrt 2D Velocity. ....	55
Table 3.26: variation in impact velocities wrt impact orientation with constant 2D velocity.....	56
Table 3.27: Dimple characteristics.....	57
Table 3.28: COR along x direction. ....	58
Table 3.29: COR along y direction.....	58
Table 3.30: COR wrt 2D Velocity. ....	58
Table 3.31: Dimple characteristics.....	59
Table 3.32: COR along x direction. ....	60
Table 3.33: COR along y direction.....	60
Table 3.34: COR wrt 2D Velocity. ....	60
Table 3.35: Dimple characteristics.....	61
Table 3.36: COR along x direction. ....	62
Table 3.37: COR along y direction.....	62
Table 3.38: COR wrt 2D Velocity. ....	62
Table 3.39: Dimple characteristics.....	63
Table 3.40: COR along x direction. ....	64
Table 3.41: COR along y direction.....	64
Table 3.42: COR wrt 2D Velocity. ....	64
Table 3.43: Dimple characteristics.....	65
Table 3.44: COR along x direction. ....	66
Table 3.45: COR along y direction.....	66
Table 3.46: COR wrt 2D Velocity. ....	66
Table 3.47: Dimple characteristics.....	67
Table 3.48: COR along x direction. ....	68
Table 3.49: COR along y direction.....	68
Table 3.50: COR wrt 2D Velocity. ....	68
Table A.1: Abbreviations.....	83

# Chapter 1

## Introduction

This Master of Science Thesis study aims to develop a numerical model of Ultrasonic Shot Peening considering single impact of shot and validating it with experiments. Ultrasonic Shot Peening is a type of Shot Peening, where particles impact on substrate surfaces with different impact angle and different velocities. This operation enhances the mechanical properties of materials at surface layers. This is due to the bombardment of small shots causing Severe Plastic Deformation (SPD) and increased residual stresses as a result of SPD. Thus, the treated material has improved surface hardness, fatigue strength and resistance towards wear and corrosion [1-4]. Several articles demonstrate the impact angle effect of peening media on roughness of the treated substrates. This is therefore determined to find out corresponding dimple characteristics and restitution coefficient by changing input impact orientation. Restitution coefficient (COR) is defined as the ratio of output shot velocity after impact to input shot velocity. This helps in determining energy loss in each shot after each impact. In addition to these parameters, effect of impact angle over single indentation geometry is also evaluated. The model developed here uses 100Cr6 steel shot over 316 Stainless Steel (SS) material. Finally, these results are interpreted with respect to experimental one and validated for consistency. Obtaining a numerical model which can take material properties, material model and machine parameters as inputs and, dimple characteristics and restitution coefficient as outputs can save a high amount of experimental duty and give the advantage of creating a data set of important parameters through complete process. Thus, the objective of this thesis study is to create a base for the numerical model of ultrasonic shot peening process considering single impacts with all of the steps included.

## 1.1 Shot Peening

A cold working process of bombarding metal and composite surface with shots is called shot peening. It results in the formation of a residual layer over the surface of the treated material. This residual layer is of compressive nature. The shots involved in this process are made up of different dimension and material. The impingement of the shots over the target surface creates a plastic deformation which in turn causes changes in the surface properties of the material which results in preventing fatigue failures, corrosion failure and increase the fatigue life of the target material[5].Figure1.1 depicts the process of shot peening as explained by Guagliano et al., [6].

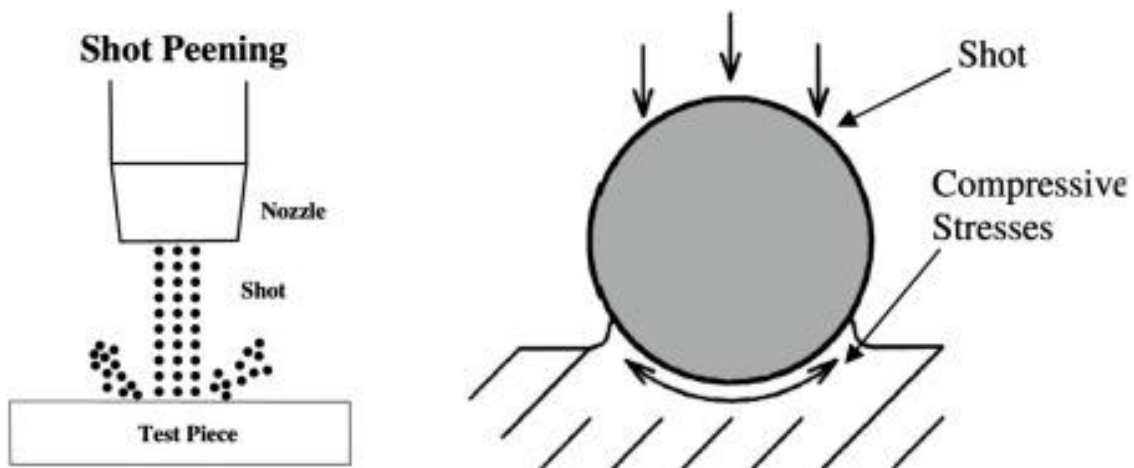


Figure 1.1 Process visualization of shot peening process

## 1.2 Principle of Shot Peening:

Principle of shot peening is that collision between the shot and target surface creates a dimple in target material which stretches the surface layer. This in turn results in formation of compressive residual stress in material surface. The compressive stress, thus formed helps in preventing the propagation of cracks[6]. The process is done usually with not a single shot but with multiple shots which results in the above said compressive residual stress. The principle behind the shot peening is depicted in the figure 1.2 as from literature [6].

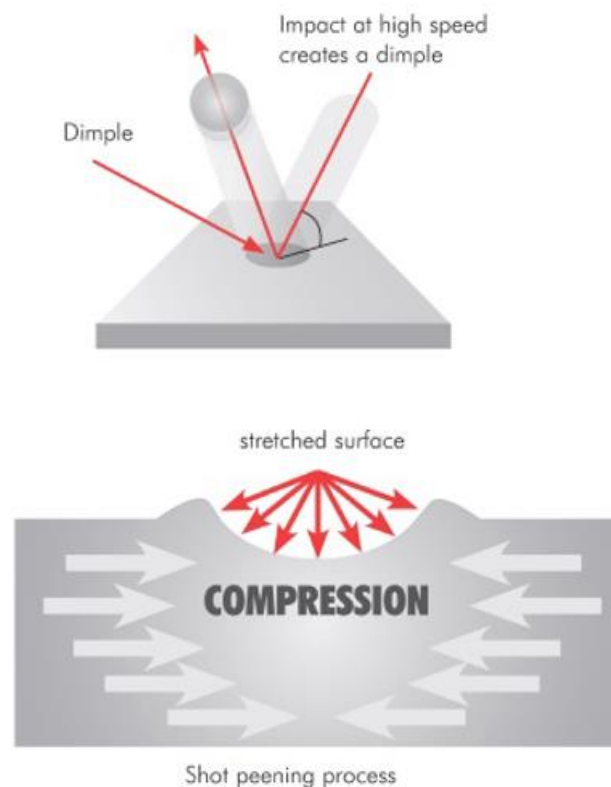


Figure 1.2 Principle behind shot peening

## 1.3 Applications of shot peening

Shot peening has found its way in various industries and it is applied to enhance the surface properties of the material and targeted at increasing the fatigue life and corrosion resistance of material. These are of primary importance in mechanical and aerospace industries. It is also useful in foundries wherein shot peening helps in producing required fine grain reformation.

Fatigue life improvement attribute of shot peening plays a vital role in aerospace industry in components such as landing gear, turbine blades. Because improvement in fatigue resisting ability aids in preventing fatigue cracking. This is made possible by introduction of compressive residual stresses which is induced on the components by the bombardment of the shots over the surface.

Shot peening extends its usefulness in automotive systems in components such as coil springs, leaf springs, torsion bars and in transmission systems. Resistance to stress corrosion cracking may come in handy in Oil and Gas Industries.

In medical field, Titanium and stainless-steel implants are treated using shot peening. This enhances fatigue life, corrosion resistance and bio-compatibility. In defence and military field, shot peening is used in treatment of armor plating.

Shot peening has also found its application in several manufacturing processes. Though there are several processes like honing, polishing, burnishing which aid in enhancement of target surface, shot peening under controlled situation aids better results. The following are some of the examples of using shot peening in different manufacturing processes from the study[9].

### Grinding:

During grinding operation, high temperature at the surfaces due to severe process, can lead to residual tensile stress and surface brittleness. Thus, produced tensile stress can affect the fatigue life of the target material. This can be neutralized by the introduction of compressive residual stress in the material. Therefore, shot peening followed by severe grinding process helps in avoiding reduction in fatigue life of a component.

Figure 1.3 depicts the distribution of residual stresses induced by various grinding techniques.

It is inferred that conventional and abusive grinding can lead to induction of residual tensile stresses which are of higher magnitude.

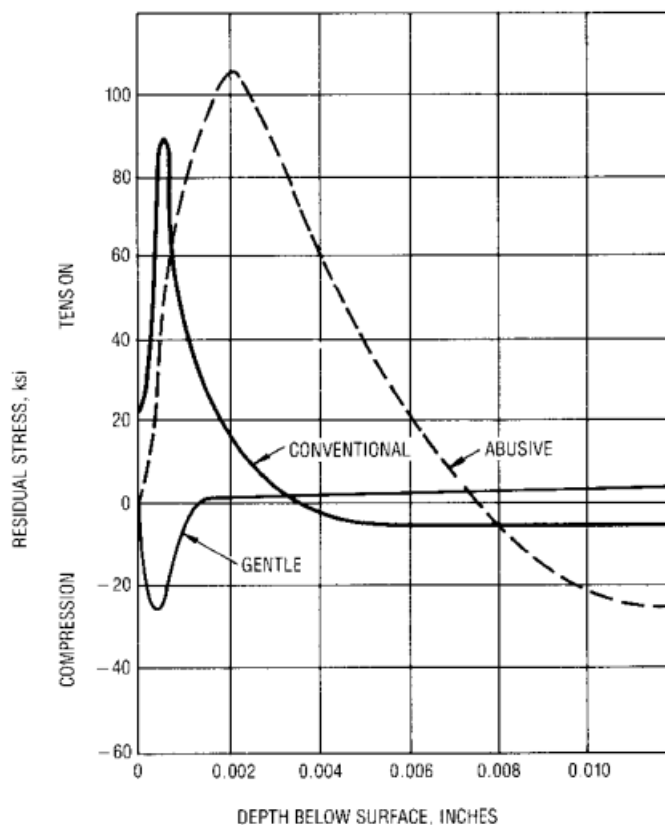


Figure 1.3 Residual Stress post Surface Grinding in 4340 Steel (Hrc50)

This affects the fatigue life of a component. This can be rectified by using shot peening which induces residual compressive stresses.

Welding:

Welding process often involves generation of heat which induces tensile stresses in the material. This tensile stress could also approach the yield strength of the target material. This stress in the heat affected zone (HAZ) may lead to reduction in fatigue property of the material. One of the ways to improve fatigue properties under such cases is by using shot peening process.

## 1.4 Ultrasonic Shot Peening

Ultrasonic shot peening (USP) is a type of shot peening technique which aids in improving the mechanical properties of materials owing to SPD induced at the surface. It is widely recognized for its ability to form a nanocrystalline or fine-grained layer on the surface of materials, which enhances properties such as hardness, fatigue strength, wear resistance, and corrosion resistance [10]. Figure 1.4 depicts the general schematics of USP Process [6].

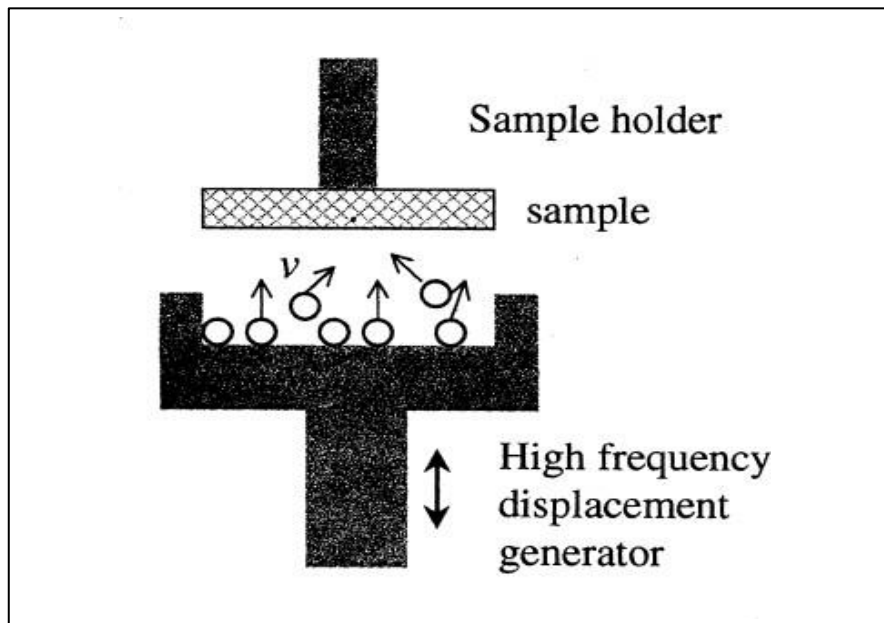


Figure 1.4 A general depiction of USP Process

A variant of peening process, USP uses ultrasonic waves of higher frequencies for accelerating small metallic shots, producing localized plastic deformation on the surface of a material which in turn results in the required mechanical properties like fatigue life [12], wear resistance, and hardness[13].

Various materials including stainless steels, have been studied for its alteration in surface characteristics owing to the application of USP, due to its ability to enhance surface characteristics without compromising bulk material properties [14].

A number of studies have been analysed with regards to ultrasonic shot peening process with various material, process parameters and its evaluation parameters are analysed [15-16].

## 1.5 Peening Parameters:

Peening process depends on different peening parameters which can be broadly classified into Material Parameters, Process Parameters and Evaluation Parameters.

### **Material Parameters**

These are the parameters that depend on shot and target material. Such parameters include the following,

1. Density ( $\text{kg/m}^3$ )

Shot Density is directly proportional to energy upon impact. This influences also the depth of the impact and stress profile of the residual stress induced.

2. Youngs modulus (MPa)

It affects stiffness of the material and therefore is indirectly related to stress profile.

3. Poisson ratio

It explains how material would deform in different direction when it is subjected to stress. Thus, it influences stress distribution and deformation under impact load.

4. Hardness

It affects the effectiveness of the shot peening process. Higher the hardness, higher the ability to induce compressive stresses in softer materials. The shot material has to be harder than the material to be impinged. Only then the deformation will be sufficient and compressive stress can be induced.

5. Yield strength (MPa)

It gives the limit up to which the deformation will be elastic. It denotes the onset of plastic deformation.

6. Ultimate tensile strength (MPa)

It denotes the ability of materials to withstand impact without fracturing. Shot peening results in repeated impacts of the shots. Higher UTS denotes better durability under repeated impacts.

## 7. Thermal properties

It is of importance since it can influence material behaviour owing to changes in temperature specifically in USP which involves high-frequency impacts.

## 8. Plastic properties

Aim of Shot peening is to induce plastic deformation which produces residual compressive stress. Therefore, plastic properties and models are of utmost importance.

## 9. Friction Coefficient

It influences the interaction between the target material and shots.

### **Process Parameters**

These are the parameters that play a vital role in performing the process of shot peening.

#### 1. Shot Velocity (mm/s)

It denotes the velocity of the shots. It influences the depth of plastic deformation, residual stress profile, final roughness of the target material and fatigue life.

#### 2. Impact frequency (kHz)

It is the number of impacts of shots over the target surface over a unit time. Greater frequency results in more frequent impacts which are shallower. It leads to a fine surface finish and potentially a greater residual stress density[12].

#### 3. Shot size and shape

As explained above, the greater the shot size greater the depth of penetration. Smaller shots induce finer surface.

#### 4. Sonotorde amplitude (mm)

It is the peak-to-peak displacement of the ultrasonic transducer's vibration. It is directly proportional to energy of impact. Increase in energy leads to increase in depth of plastic deformation and enhanced stress profile.

### 5. Peening intensity ( $J/mm^2$ )

It denotes the energy transferred to the target surface. It influences the depth of compressive stresses and plastic deformation. It also can damage the target material if applied excessively[17].

### 6. Peening time (s)

It is the time required for the peening process. After a certain limit, the rate of increase in depth of penetration increases comparatively[11]. Peening time vs roughness graph can be inferred from [4] and it is depicted in figure 1.5.

Measured  $P-V$  value of the peened plates with different peening conditions.

Peening parameter		$P-V$ value ( $\mu m$ )		
Diameter (mm)	Peening time (min)	Line 1	Line 2	Average
1.4	10	52.17	62.55	57.36
1.4	20	85.252	96.779	91.0155
1.4	30	104.79	112.55	108.67
3.9	10	99.308	81.784	90.546
3.9	20	103.017	110.396	106.7065
3.9	30	114.728	111.796	113.262
6.4	10	116.239	99.039	107.639
6.4	20	135.917	142.309	139.113
6.4	30	150.541	161.094	155.8175

Figure 1.5 Peening Parameter vs Roughness

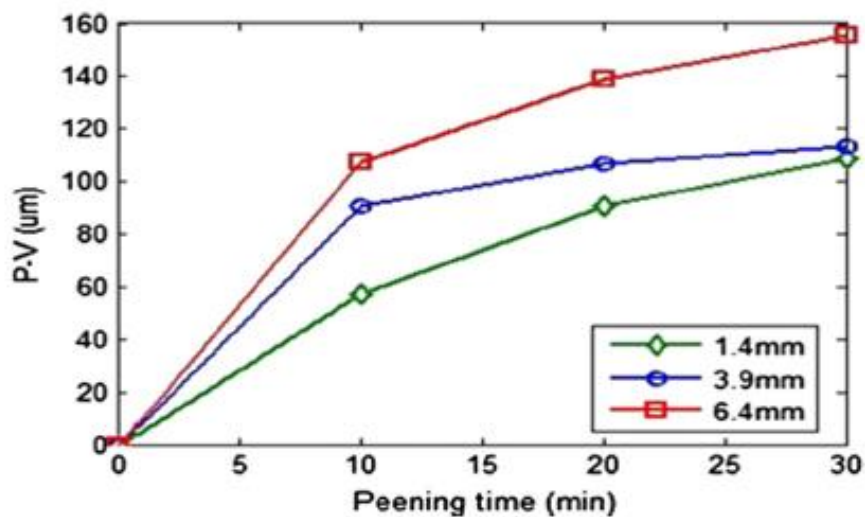


Figure 1.6 Peening time vs roughness

### 7. Impact angle

It is the angle at which the shot impinges the surface. A perpendicular angle results in maximum energy transfer and compressive stress.

### 8. Almen Intensity

It measures the peening intensity. Almen strips are used to record deflection owing the peening process. It verifies whether correct peening intensity was applied and aids in quality control for peening process.

### 9. Coverage

It denotes the percentage of surface area impinged by the shots during shot peening process. Higher coverage results in uniform stress distribution but may also lead to surface damage if it is excess as explained in the study [22].

Song et al. [23] depicts the variation in PEEQ (Equivalent Plastic Strain) and variation in residual stress value from surface level with respect to a particular impact velocity and variation in coverage. It is affected by angle of impact, impact velocity and standoff distance. It is evaluated analytically usually by using Avrami equation. It affects the residual stress gradient and PEEQ.

The Figure 1.8 and 1.9 from Song et al. [23] depicts the variation in PEEQ and variation in residual stress value from surface level with respect to a particular impact velocity and variation in coverage.

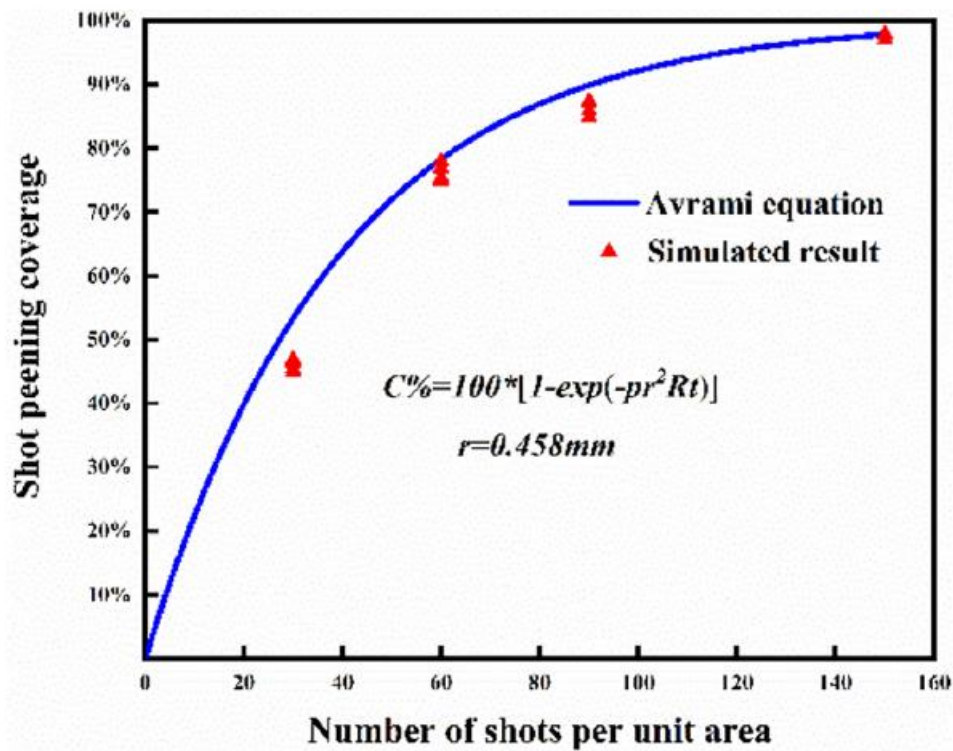


Figure 1.7 Coverage in terms of number of shots per unit area

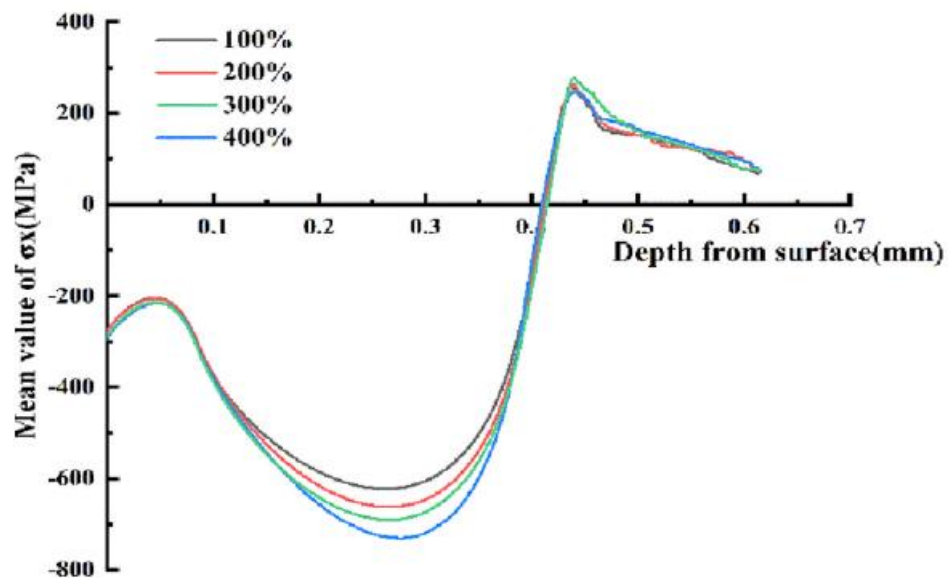


Figure 1.8 Variation of the RS gradient as the coverage changes

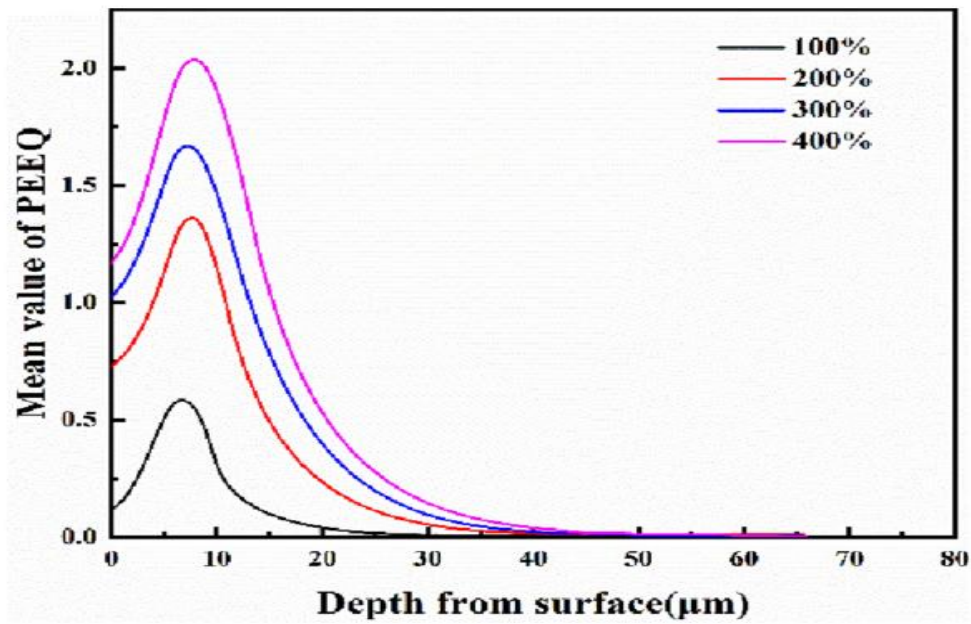


Figure 1.9 Variation of the PEEQ gradient as the coverage changes

### Evaluation parameters

These are the parameters which are used to inspect and attribute the shot peening process.

#### 1. Residual stress profile

It denotes the distribution of compressive residual stress induced by shot over the target material. It is of the primary target of shot peening process as it helps in enhancing fatigue life of the material[18-19].

#### 2. Surface Hardness

It denotes the hardness of the material after impacted by the shots in shot peening. If this parameter is increased in comparison with the initial one, then it indicates that the plastic deformation is effective.

### 3. Surface roughness

It impacts the following; materials fatigue life[20], corrosion resistance and surface finish [21]. Fatigue life can be improved using USP by the introduction of compressive residual stress. Thus, formed stresses counteract the tensile stress that leads to crack growth. Less plastic deformation takes place in harder materials and this results in fine-tuned reduction in roughness and in the other case, softer material will be more prone to maximum deformation that results in rougher finish. Therefore, an optimum balance is required for maximizing fatigue life while keeping surface roughness in a manageable range.

### 4. Peening depth (mm)

It denotes the depth in the target material up to which the material properties were changed. It plays a vital role in the fatigue life and surface durability of the target material.

### 5. Fatigue life improvement

It is one of the main attributes of shot peening process[24-26] since the formed layer of compressive residual stress acts as a protective layer against formation of fatigue cracks which have the tendency to form under tensile stresses.

## 1.6 Principle of USP

The following are the mechanism behind USP process. Material parameters and process parameters are determined. The spherical shots are placed in a reflecting chamber which also includes ultrasonic concentrator. Ultrasonic generator produces vibration which causes the shots to vibrate by a mechanical system and connection of a generator, a piezoelectric transducer and a booster. Usually, the frequency of the ultrasonic system can be up to 20 kHz. Piezoelectric electrical emitter aids in converting this electrical signal to mechanical signal. Amplification of this created mechanical signal is possible with the help of the sonotrode and some boosters. This amplified signal is then transferred to the shots which impacts the target surface. The shot that impacts the surface might also impact the target again after rebounding. This may lead to change in angle of impact and also the collision between the shots before or after collision may also lead to change in impact orientation. Figure 1.10 [45] depicts the schematics of USP Principle.

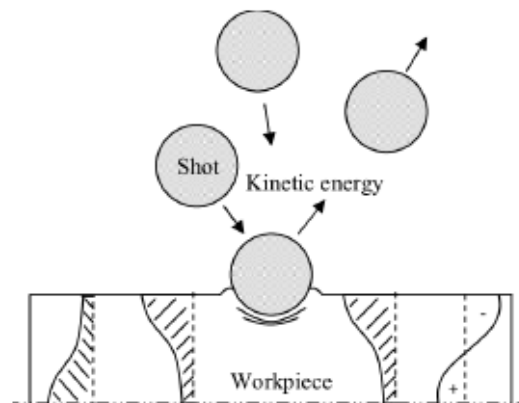


Figure 1.10 USP Principle

## 1.7 Attributes of Ultrasonic Shot Peening:

- Enhancement of Fatigue life

Some of the aerospace components like turbine blades and landing gears can be subjected to fatigue failure owing to cyclic loading. In such cases, USP aids in enhancing fatigue life of those components. This is possible due to the introduction of residual compressive stress which delays crack initiation and therefore delaying crack propagation[26].

- Reduction in Weight

Improvement of surface integrity can lead to reduction of weight of the component used in an application without the need to compromise for the strength [6].

- Resistance to wear

Components such as crank and cam shafts can be subjected to USP to increase wear resistance. Hardening induced by the peening operation enhances the performances of the above said parts which are subjected to extreme loads and temperature [12].

- Surface Hardening of Medical Devices:

Components used in medical implants are subjected to wear and fatigue. Their lifespan can be improved by using USP. Studies have shown that implants treated with USP has experienced less wear and improved biocompatibility. Thus, it proves their suitability in medical applications.

- Stress Relieving

USP introduces compressive residual stresses as explained by Guagliano et al.[12] on the surface of the material where it is impacted. Therefore, if a material with initial tensile stress accumulated is used for treatment, USP helps in relieving those residual tensile stresses accumulated in components.

- Corrosion resistance

Introduction of residual compressive stresses and refinement of surface aids in reduction in stress-corrosion cracking [9].

- Surface Enhancement and creep resistance

USP helps in enhancing surface properties of the target material owing to repeated impacts over its surface [10].

## 1.8 Comparison between CSP and USP

Conventional shot peening and ultrasonic shot peening differ from each other in few aspects. Most of these differences are observed in evaluation parameters discussed above. They are surface roughness, stress profile, surface hardness. They also differ in process parameters such as shot size, shot velocity and impact direction.

It is concluded that when used under similar conditions and parameters, air blast CSP produces greater volume of structure which are nano-crystalline [12]. The following table from the above literature depicts few of the differences.

	Air-blast shot peening	Ultrasonic shot peening
Shot size (Diameter - mm)	0.05,0.3	0.4
Shot velocity	>100 m/s Distribution is small	<20 m/s Distribution is large
Impact direction	Single direction	Multiple direction

Table 1.1 Comparison of pneumatic CSP and USP

The size of shots used in CSP is limited while those used in USP are not limited. This is because one can use a shot which is as large as several millimeters in USP.

This ensures that the energy delivered per impact to the target surface by the shot is larger in USP than in CSP. Though the velocity is low, this shot dimensions ensures that the energy per impact in CSP is lower than USP. Since depth of hardened layer depends primarily on energy per impact and not on the number of impacts, it can be concluded that USP has better depth of penetration compared to CSP.

Another important difference is that impact direction in CSP is unidirectional which is perpendicular to the target surface. But in USP, impact angle is not unidirectional. This can be attributed by the secondary and further impacts of rebounded shots and also owing to the collision between the shots. Thus, this study aims in analyzing the given condition with variable angle of impact.

## 1.9 Literature review on Numerical Model of Ultrasonic Shot Peening

Several studies have been undertaken with various purpose using numerical modelling of shot peening process. Aim of the review for this study is to focus on studies involving determination of surface roughness and variation with respect to several target and shot material while the inputs being shot impact velocity, angle of orientation and material parameters.

In this study, the peening media used is 100Cr6 steel shots, a high-carbon chromium-bearing steel known for its excellent hardness and wear resistance. The target surface to be bombarded with shots is 316L Stainless Steel. Model used for modelling plastic deformation is Johnson-Cook model. Improving the surface properties of the target material with steel shot can enhance its performance in demanding environments.

Miao et al. [41] studied on Finite element simulation on Shot peening. It focused on Finite Element simulation of shot peening. It simulated the actual peening process. This model has the ability to simulate the multiple impacts with the minimum model size. The influences of parameters such as shot type, shot size and shot impact velocity is studied through the model. It aims over random impact locations for a sequence of impacts rather than having a single impact angle. This helps in our study of analysing system with different impact angles and velocities. In our study the shots are impacted in different angles onto the surface of the substrate and the effect of different impact angle is made possible through varying velocity of the shot in x and y direction and evaluation parameters are analysed. The idea is to relate these input parameters for a single shot impact and analyse the dimple characteristics and COR.

Bagherifard et al. [20] focused on developing numerical model of shot peening process using a shot with various velocity such 30,60,90 and analysed the results with experimental one. The 3D finite element model developed in this study helps in predicting the surface topography alterations in target material as a function of peening parameters and processing time. The same model could be used as the base for this study considering single impact and change in 2D Velocity.

Badreddine et al. [27] progressed their research in studying Ultrasonic Shot Peening process through a detailed 3D Numerical Model of the shot and target specimen and verifying its relevancy with experimental data. It helps in determining the output velocity and impact velocity in an experimental way. Thus, aiding in determining shot trajectories and optimizing the 3D Numerical Model.

The study by Hong et al. [19] provides a computational model of the shot peening process, where a FEM was utilized in understanding the dynamic process of the shots which impinges on the target material in the process. The study used Discrete Element Method like several other studies in order to predict the multiple particle dynamics. The model established relationship between various peening process parameters and the evaluation parameters and regulates control over these parameters.

Li et al. [11] helps in predicting the surface nano crystallization in carbon steels using numerical modelling of the ultrasonic shot peening process. It helps in correlating different process parameters to the results of the process such as indent depth and indent diameter.

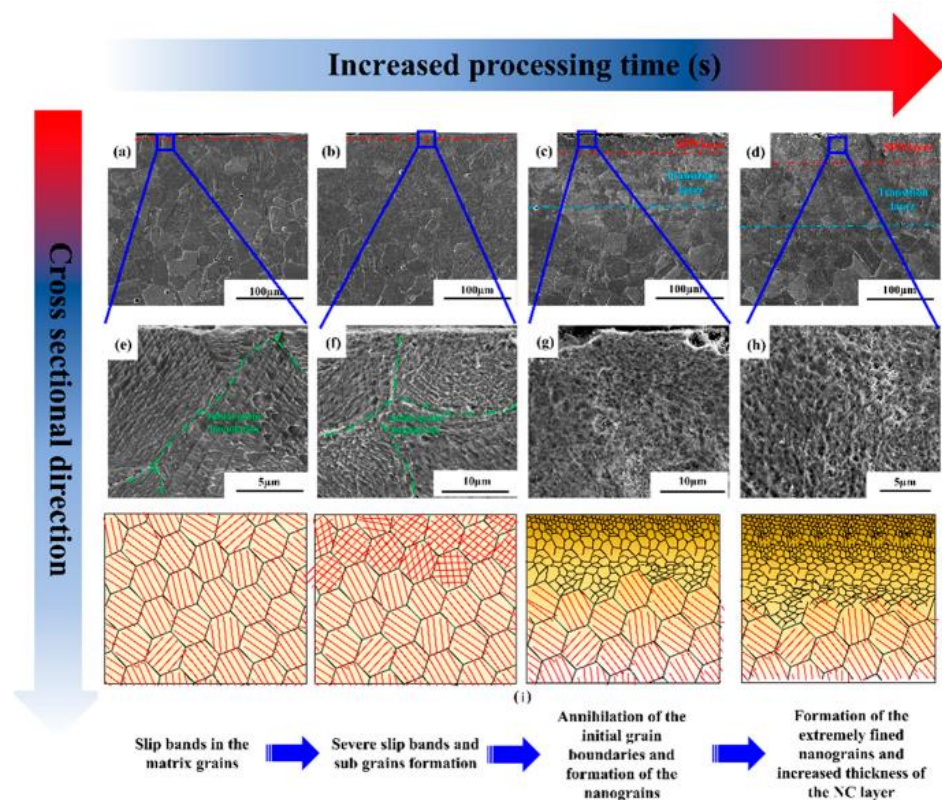


Figure 1.11 Attributes of Shot peening over grain reformation

Figure 1.11 from Li et al. [11] explains that the peening time has a direct influence over the depth to which surface treatments occur. It could be inferred that the intensity of the impact during the ultrasonic shot peening process can be significantly improved by increasing the amplitude of the ultrasonic tip and frequency of the ultrasonic signal, as well as by decreasing the working distance from the target surface to the ultrasonic tip.

Yin et al. [4] also relates various process parameters to surface topography of the target material. It provides the numerical model of ultrasonic shot peening for low carbon steels. It interprets the relation between peening time and grain size and indent thickness and the relation between strain rate and plastic deformation (by twinning on top surface) and grain size.

The objective of this thesis is to conduct numerical simulations of singular impacts during ultrasonic shot peening with different impact angles while using a material model that is validated in terms of induced plastic deformation by investigating the dimple geometry under a  $90^\circ$  impact both numerically and experimentally.

Initially, papers regarding 316L were studied to determine its effects after the impact of the shot [28]. Material model for 316L material is determined after reviewing various studies which helped in determining the differences between Johnson-Cook Model [29] and Cowper-Symonds model[30].

The following papers helped in determining the material model when it is subjected to various deformation and heat treatment processes.

Gao et al. [31] and H. Li et al. [32] analyses microstructural evaluation and deformation behavior in steel mainly 316L Stainless steel with respect to different plasticity models. These studies helped in differentiating these models and the differences between the above two models with respect to different criteria are discussed as follows.

### 1. Formulation

Formulation for Johnson cook model included the effects of strain rate, strain, Temperature and pressure. While Cowper-Symonds model included only Strain rate and temperature.

### 2. Materials

The Johnson cook model is used mostly for Metals and Alloys while the Cowper-Symonds model gives more accurate value for ductile materials.

### 3. Applicability

The Johnson cook model is used in high strain rate events like Impacts and Penetration while the Cowper-Symonds model is used in events where determination of dynamic behaviour is important.

### 4. Strain rate sensitivity

Johnson-Cook model is more intricate than Cowper Symonds model with respect to strain rate sensitivity.

### 5. Computational efficiency and accuracy

Johnson-Cook model is complex and more accurate. But its accuracy depends on the parameters used. While Cowper Symonds Model is simple and comparatively less accurate.

Since we need a model with better accuracy and a model suitable for high strain events like impacts, Johnson-Cook model is used for this study. Once the material model feasible for this study is determined, literature review scope is narrowed down to the target material – 316L Stainless Steel. Johnson-Cook parameters of the target material is determined through various studies.

Studies of Aberbache et. [33], Ebrahimi & Hermans [34] and Rahman Chukkan et al. [35] helped in determining the Johnson-Cook parameters for 316L Stainless Steel.

These papers involved various deformation treatments and processes on 316L Stainless steel and the corresponding results with respect to different plasticity model parameters. Those parameters for this study are obtained from Philip & Chakraborty [29] and also Tamer et al. [42] helps in analyzing Johnson-Cook parameters for 316L Stainless Steel.

Finally, crucial Johnson-Cook Parameters such as Initial Yield Strength (A), Strength Coefficient (B), dimensionless strain rate hardening coefficient (C), Strain Hardening Exponent (n), Thermal Softening Coefficient (m) are determined[36]. Once the material Parameters are determined, its influence over numerical simulation is studied.

Sanjurjo et al. [37] analyses the effect of the constitutive material model which describes the substrate material on the results yielded from numerical modelling of shot peening process. The effectiveness of each constitutive model is analyzed by comparing the numerical predictions of residual stress and roughness with the experimental findings. Process parameters were then taken into account for the study.

Badreddine et al. [15] aids with a study on model predicting the dynamics of the shot and influence of initial conditions over it. The model is then utilized to determine predictive values of the spheres before the impacts. The influence of the ultrasonic shot peening parameters is also evaluated.

Considering the parameter included in the study, a numerical model is simulated. Prior to the simulation, several studies were taken to correlate numerical simulation with different parameters to experimental ones.

Bagherifard et al. [38] focused on creating a numerical model of the shot peening process. It aimed in predicting treatment conditions after the process with the aid of accuracy in the model in terms of mesh parameters and constitutive law of the material. It involved multiple impacts of shots over the target surface.

Chen et al. [39] provided the literature review on numerical modelling of USP process and optimising these parameters in order to get the required surface treatment. It predicted the effect of angle of impact and impact velocity for optimizing the peening process.

Yin et al. [40] determines the generation of nanostructured surface layer by plastic strain, an analytical algorithm cooperating with finite element method and aided in simulating strain distribution and surface topography of the peened surface during USP.

Simulations like Finite Element Analysis has been used in this study to predict the mechanical behavior of 100Cr6 steel under different peening process parameters, thus helps in analyzing the residual stress profiles and surface deformation.

The parameters used to determine the plastic deformation on the target surface after a single impact is depicted in the figure 1.12 and they are as follows:

1. Depth of the Dimple
2. Width of the Dimple

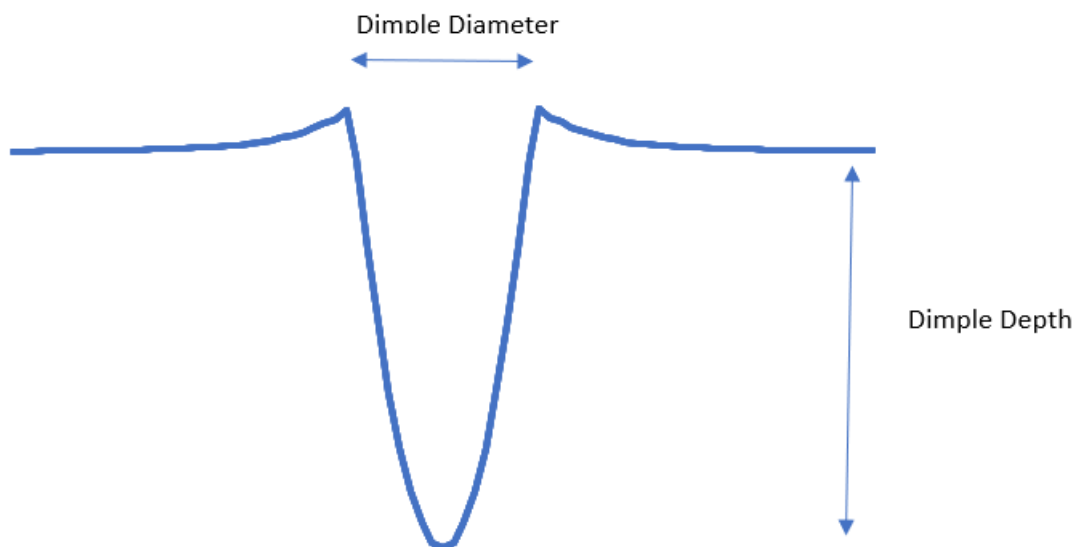


Figure 1.12 Schematics of a dimple

Depth of the dimple denotes the depth of penetration and width of dimple denotes the surface impinged a single shot. Greater the depth of penetration depicts the depth of microstructural changes happening in the material owing to the impact as explained by Ganguly et al. [10].

Ganguly et al. [10] evaluates the effects of shot peening process and parameters over the surface topography. It explains the variation in indent depth with respect to change in peening time. Whenever the time is increased the indent depth is increased. The Figure 1.13 from [10] depicts that increasing the USP Peening time increases the indent depth and surface roughness. It also shows its effect in AZ91 Alloy with different Graphene nanoplatelets content.

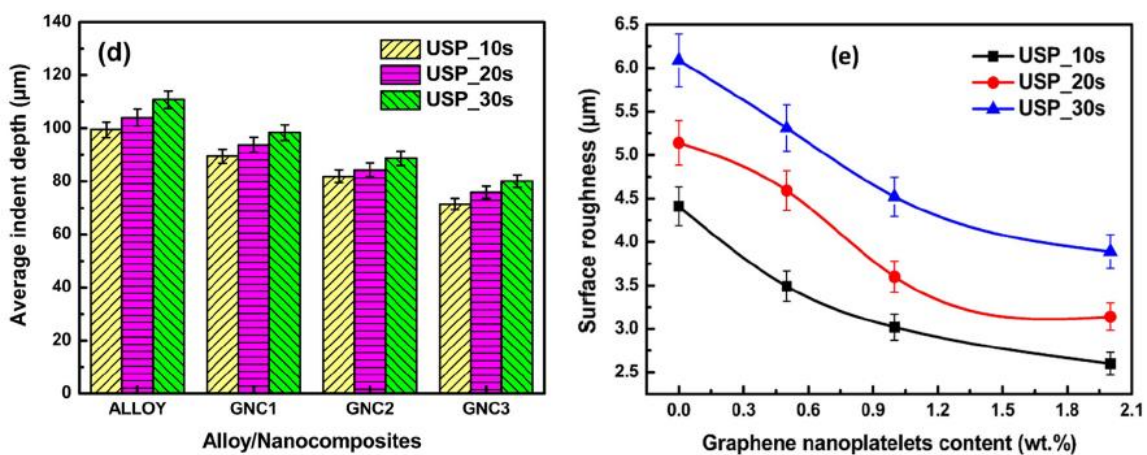


Figure1.13 Indent depth and Surface roughness vs Peening time (Alloy)

Another crucial factor considered in this study is the Coefficient of Restitution (COR), which helps in determining energy losses during an impact. It plays a vital role in determining how efficiently the energy is transferred from shot to the target material during an impact. Thus, it affects the depth and diameter of the dimples created during impact.

Badreddine et al. [27] aids in providing a numerical model of USP as discussed above. It helps in determining the impact and output velocity of the shots and helps in determining the relation between the Restitution coefficient and the surface characteristics.

The above-mentioned study by Badreddine et al. [15] have investigated the role of the restitution coefficient in shot peening and its influence on change in surface characteristics. This study aims in calculating the coefficient of restitution in a numerical way and determine the energy losses during an impact.

In addition to shot velocity and restitution coefficient, influence of orientation of shots over dimple width and dimple depth is also analyzed.

The angle at which shots impact the material surface can significantly influence the surface characteristics of the impacted surface. Such variation in orientation is due to secondary impact of shots or / and collision between the shots. These variations in orientation are often overlooked in simulations, but recent studies have shown that controlling shot orientation leads to more uniform surface treatment and improved material properties. These different parameters influence the surface features of the target material.

## 1.10 Challenges and Solutions

This study faces several challenges, in specific with accurately simulating impacts with different impact angle and incorporating material properties in the simulation which varies with respect to shot orientation and velocity. The dynamic nature of ultrasonic shot peening, combined with the material behavior of 100Cr6 Steel, requires precise simulation models and boundary conditions.

These issues could be taken care through the usage of advanced FEA simulations which aids in modelling the dynamic impact of 100Cr6 Steel Shot over 316L Stainless Steel at varying orientations. The synergic effect of the impact velocity and impact angle can be regarded as a future study.

This approach provides a comprehensive understanding of how different shot impact angles and corresponding changes in velocities influence the surface properties of 316L Stainless steel, contributing to the development of more efficient shot peening processes for high-performance components.

## Chapter 2

# Numerical Model Build-up

### 2.1 FEA Model for USP

A numerical model depicting single impact of shots considering all the parameters has been created. Several studies involving Ultrasonic shot peening over target material were studied as explained in section 1.9.

#### **Abaqus FEA Model**

For Finite Element Analysis (FEA), ABAQUS Dynamic/Explicit is used. Different modules in the numerical simulation are explained as following and the specificity in modelling with different parameters are explained in section 2.2;

#### **1. Part Module**

Target substrate and shot with specific dimensions are created. Appropriate face partitions and cell partitions are used in the parts. This helps in achieving the required meshing in the Mesh Module.

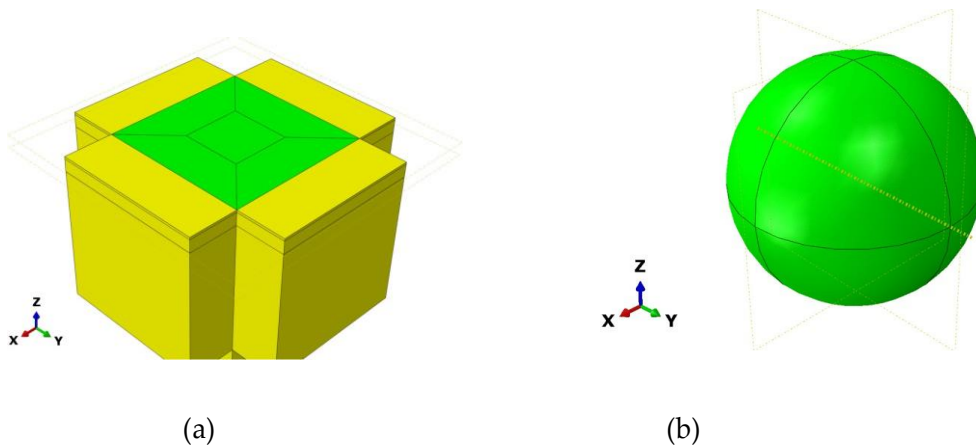


Figure 2.1 Target (a) and shot Model (b)

The shot and target parts modelled in FEA software are shown in the figure 2.1. The diameter of the shot used in this study is 2mm.

## 2. Property Module

In the following study, both the target and shot material is steel. Difference in their hardness makes it possible for using 100Cr6 over 316L Surface. The shot material used here is harder than the target material. This ensures that the material under impact deforms plastically while the shot material remains undeformed. This results in a uniform distribution of compressive stresses on the target surface, improving fatigue resistance, wear properties, and overall durability of 316L in demanding environments. The following are the inputs required in property module;

### Shot

Density (kg/mm<sup>3</sup>), Yield strength (MPa), Poisson ratio.

### Target specimen

In addition to above-said Elastic parameters, parameters due to plasticity of the target material are used.

Owing to the impacts of the shots, the target material gets deformed plastically and therefore plasticity of the target material has to be taken into consideration. Various articles regarding Plasticity models were studied as explained in the section 1.9 and Johnson-Cook Model is used in this simulation owing to its advantages in high strain rate sensitivity and accurate results over other models for a particular material.

Johnson-Cook material model is given by the equation below;

$$\sigma = [A + B\epsilon^n] \cdot \left[ 1 + C \ln \frac{\dot{\epsilon}}{\dot{\epsilon}_0} \right] \cdot \left[ 1 - \left( \frac{T - T_0}{T_m - T_0} \right)^m \right] \quad (2.1)$$

This equation 2.1 can be divided into three parts depending upon their contributions.

The first part,  $[A + B\epsilon^n]$  denotes

A - Initial Yield of the material (MPa),

B - Flow stress on strain hardening (MPa),

n – Strain hardening exponent

These data can be obtained using stress-strain curve given for a particular strain rate. This particular strain rate is the reference strain rate ( $\dot{\epsilon}_0$ ) for the entire model.

The second part is due to contribution of strain rate dependency. It considers interpreted data of stress-strain data of the material under various conditions of strain rate ( $\dot{\epsilon}$ ). Ultrasonic shot peening leads to occurrence of higher strain rates. Thus, the model used to characterize the plasticity of the material must incorporate data related to higher strain rates. Hence, the validity of the model for higher strain rates is ensured. The parameter used in this contribution is strain rate sensitivity (C).

The third and the final contribution corresponds to temperature effect. Stress-strain data of a material can be affected or changed by change in temperature. Thus, it is included in the model to increase the accuracy of the model. The parameters under this contribution are obtained from stress-strain data of a material under different conditions of temperature (T).

They are;

m - Thermal softening parameter

$T_m$  – Melting temperature of the material under consideration (K)

$T_0$  – Reference temperature / Glass transition temperature of the material (K)

### 3. Assembly Module

In this module, both the parts (shot and target) are assembled together. The shot is placed above the target material. A contact point is formed upon interaction and it is placed exactly at origin for simplicity. The following figure depicts a general representation of the Assembly module used in the simulation.

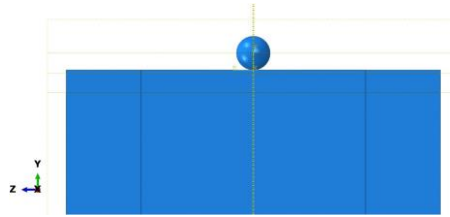


Figure 2.2 Generic representation of Assembly Module

### 4. Step Module

Dynamic/Explicit is arranged with a total step time as  $1 \times 10^{-5}$  s. Some of the simulations with lower velocity are run with a step time of  $1.5 \times 10^{-5}$  s so that sufficient time is available after impact to determine the output velocity of the shot after impact. Outputs are taken at each time zone of  $2.5 \times 10^{-6}$  s. This periodic interval in step helps in determining the output velocity of the shots.

### 5. Interaction Module

For the analysis, a general contact has been given. In addition to it, a penalty of frictional coefficient is also included. Value of frictional coefficient used in this study is 0.2.

### 6. Load Module

Impact velocity of the particle is the only load applied in the entire simulation. It is defined as a predefined field. It is assigned to shot particle on the negative axes of Y direction. This is to ensure that the shot is moving towards the upper surface of the target material considered.

## 7. Mesh Module

Meshing section of the simulation involved both 3D Stress Elements and Acoustic Elements. Side walls of the target material are meshed with Acoustic elements. The region that remain between those side walls and the entire region of the shot part are meshed using 3D stress elements.

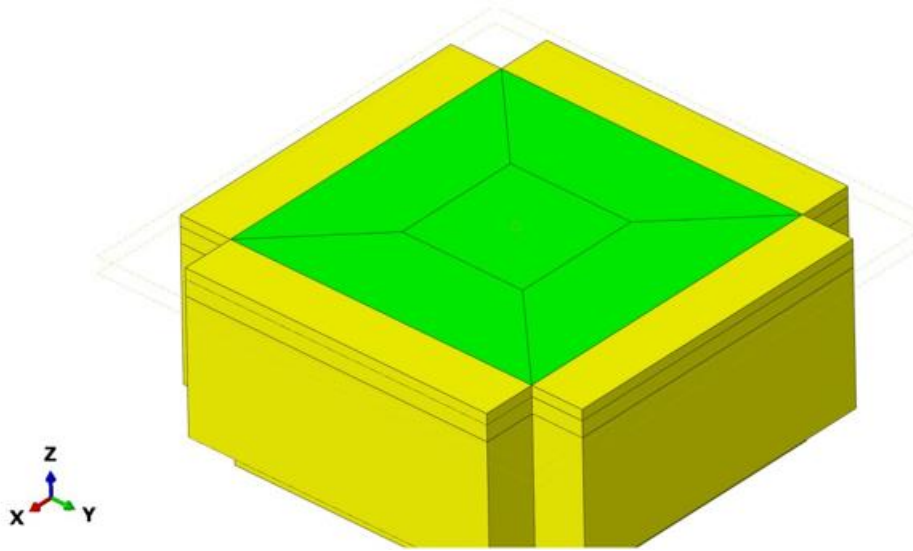


Figure 2.3 A generic representation of Acoustic elements in Mesh Module

3D stress element that is used here is C3D8R . These elements are 8-node linear brick, reduced integration with hourglass control. The meshing size used in this study is 15 micrometer in the impact zone which needs to be characterized by a fine mesh for an accurate depiction of plastic deformation.

In order to prevent reflection of stress waves back into the system, Half-infinite meshes are needed. The real reason behind the usage of acoustic elements is to replace them with such Half-Infinite meshes. This is made possible by making changes in input file of the simulation.

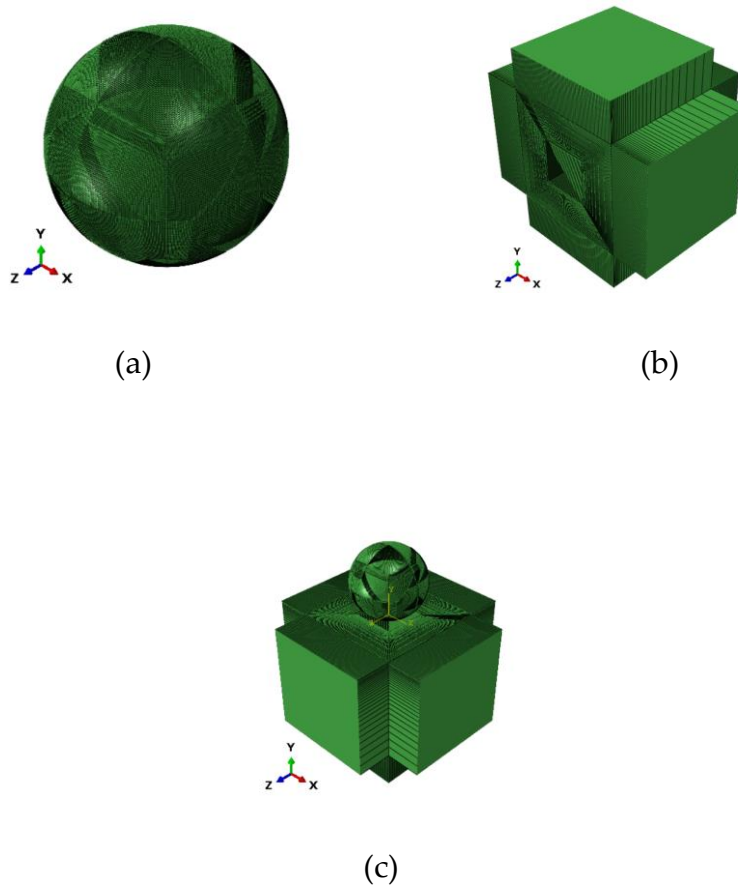


Figure 2.4 A generic representation of meshing Module

Once the meshing is done, job is created and input file for the simulation is written. Then file is edited by replacing Accoustic elements (AC3D8) using Half-Infinite Elements (CIN3D8). It is done because there were no boundary conditions set to the substrate walls which may lead to inaccurate results. After replacing the elements of the side walls, the input file is uploaded into FEA Software as input. Thus making the simulation ready for job submiting and analysis.

## 8. Job Module

A job is created and submitted and then the simulation is analysed for single impact of shot over the target surface. The simulation is repeated for various angle of impacts and velocities and results are recorded.

## 2.2 Simulation characterization

### 2.2.1 Target material characterization

The target material used in the study is 316L Steel. The reason for choosing this material over several other is due to its widespread industrial applications. Therefore conducting a numerical simulation of 316L stainless steel and optimising the process for different velocities and different orientations can benefit in widespread usage.

316L stainless steel has found its place in industries like aerospace, medical devices, and also in food processing industry owing to its biocompatibility, corrosion resistance, and strength. Hence, using 316L as the target material provides relevant insights that can be directly applied to these industries, making the findings of this study more impactful.

The material parameters of the target material were studied and its influence over ultrasonic shot peening process is analysed upon various simulation conditions.

The density and elastic material properties are obtained from the research papers mentioned in section 1.9 and Granta Edupack Software was also used to validate the range of values for these properties. The table 2.1 provides such properties of the target material considered for the simulation.

Material / Properties	316L Stainless steel
Density (kg/mm <sup>3</sup> )	7.8E-09
Yield Modulus (N/ mm <sup>2</sup> )	210000
Poisson ratio	0.3

Table 2.1 Density and Elastic Properties of the target material

Since the shot impacts the target material, plastic deformation occurs in the target material. Thus a plasticity model is considered to determine the plastic properties of the material under consideration. Johnson-Cook model for 316L is studied under several deformation processes. These studies helped in determining the parameters of Johnson-Cook model. Those parameters obtained from Philip & Chakraborty [29] are represented in the table 2.2.

Material / Parameters	316L Stainless steel
A (MPa)	250
B (MPa)	1143
n	0.67
m	1
T <sub>m</sub> (K)	1820
T <sub>0</sub> (K)	300

Table 2.2 Parameters of Johnson-Cook Model

### 2.2.2 Shot material characterization

The shot material used in this simulation is 100Cr6 steel shot. The shot material does not plastically deform and therefore only elastic properties are required.

Higher hardness comparable to the target and higher impact resistance are the main requirements for the shot material to produce dimple in the target material and to have higher process efficiency.

Therefore, using 100Cr6 as the shot material ensures optimal peening efficiency, consistent surface treatment, and durability of the shots, making it a preferred choice for ultrasonic shot peening on target materials like 316L stainless steel.

Only the elastic properties of the shot are required. Granta Edupack software is used as reference to determine ranges of those properties and several studies involving steel shots are studied to determine these properties.

Material / Properties	Steel
Density (kg/mm <sup>3</sup> )	7.8E-09
Yield Modulus (N/ mm <sup>2</sup> )	210000
Poisson ratio	0.3

Table 2.3 Density and Elastic Properties of the Shot material

### 2.2.3 Validation of Material model

Once the material model is determined, a simulation is run at normal velocity of 3600 mm/s and at an impact angle of 90 degrees. This is done in order to compare the results from numerical model with experimental data available at those process parameters.

The experimental data is shared by LEM3 laboratory of University of Lorraine located in Metz, France as part of the active collaboration with Arches Lab in Politecnico di Milano. Single impact experiments are done on a specific equipment as shown in Figure 2.5. In particular, a single shot is placed inside the equipment and a pressurized air is fed into the system, as the main accelerator media for the shot. The air-shot stream leaves the nozzle and impacts the substrate surface that is fixed on the other side of the machinery. A high-speed camera is placed on the top of the equipment, allowing for top view for tracking the shot trajectory. This allows for gathering the images both before and after the impact. Computing the distance between shot positions at consecutive frames along with the imaging frequency of the system leads to accurate evaluation of corresponding velocity values.

Data at 90 degree	Experimental Data	Data from Numerical model	Discrepancy (%)
Dimple Depth (mm)	0.010	0.008	20
Dimple Diameter (mm)	0.309	0.270	12.6

Table 2.4 Validation of material model

Since the discrepancy is within the accepted range, the parameters used for plasticity model is validated and used for the various simulation cases in this study.

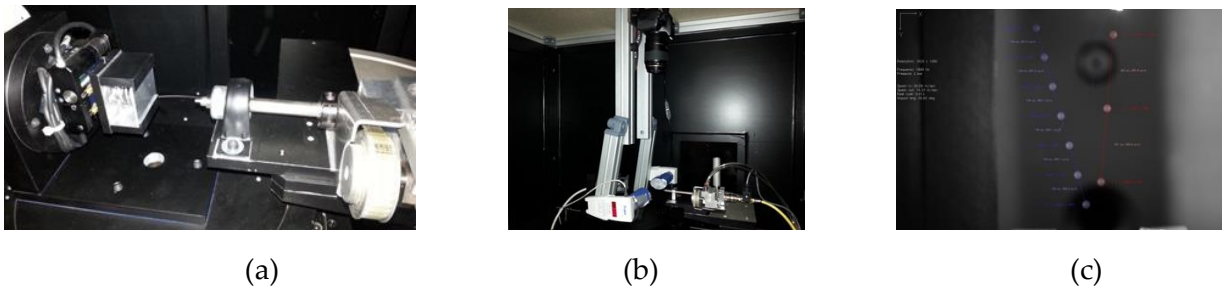


Figure 2.5 Equipments for experimental analysis

### 2.2.4 Shot velocity and orientation characterization

Once the Material parameters and process parameters (except impact orientation and impact velocity) are fixed, the simulation is iterated for several values of impact orientation and impact velocity and the results are analysed. The simulation is executed at 2 different cases. Velocities only along x and y direction is considered in this study to determine the variation of dimple diameter, dimple height and restitution coefficient with respect to change in the angle of impact.

#### Case 1

The simulation is iterated at same normal velocity ( $V_y = 3600$  mm/s) but different 2D velocity. In this study, Normal velocity is the velocity along the y direction which is perpendicular to the target substrate. The variation in 2D velocity is owing to the change in impact angle of the shots.

#### Case 2

The simulation is iterated at same 2D velocity but at different normal velocity. Here, the 2D velocity,  $V = 3600$  mm/s and the variation in  $V_y$  is possible due to change in impact direction (impact angle).

The angles considered for evaluation are  $90^\circ, 75^\circ, 60^\circ, 45^\circ, 30^\circ, 15^\circ$ .

### 2.2.4.1 Relationship between 2D Velocity and Angle of impact

Consider a 2D Velocity vector,  $V$  that can be decomposed into 2 components as follows,

$V_x$  - Velocity in X direction

$V_y$  -Velocity in Y direction

Figure 2.6 shows how a shot impinges the target substrate. Let  $\theta$  be the angle at which the shot impacts the target.

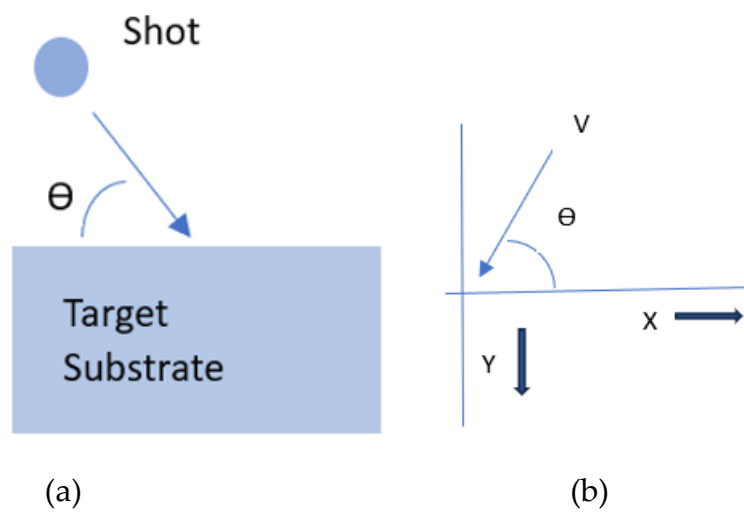


Figure 2.6 Depiction of 2D Velocity Vector

Therefore, the magnitude of 2D Velocity vector is given by,

$$V = \sqrt{V_x^2 + V_y^2} \quad (2.2)$$

And also,  $V_x$  and  $V_y$  can be determined by knowing angle  $\theta$  and magnitude of  $V$ .

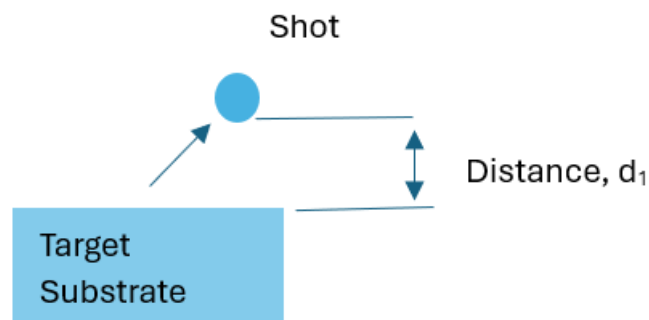
$$V_x = V \cdot \cos \theta \quad (2.3)$$

$$V_y = V \cdot \sin \theta \quad (2.4)$$

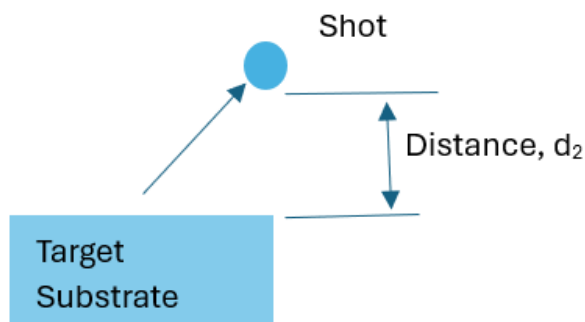
### 2.2.5 Step time Characterization

One of the inferences from the study is to determine Restitution coefficient in different directions. The restitution coefficient is determined by determining the distance between the target and the shot after impact and calculating the time to reach that distance produces the output velocity of the shots.

The restitution coefficient is determined by the ratio of output velocity of the shots to the input shot velocity. Thus, step time plays a vital role in determining COR. Sufficient step time has to be allocated after the impact so that it is feasible to determine the step time taken by shot to bounce back to a particular distance after impact.



(a)



(b)

Figure 2.7 Graphical Representation for determining COR in the normal direction to the substrate surface

The lower mid node of the spherical shot and top mid node of target is taken as a reference. Distance is measured between the lower mid node of shot and top mid node of the target. This distance is tracked between successive step times  $t_1$  and  $t_2$  which is represented as  $d_1$  and  $d_2$ .  $d_1, d_2, t_1$  and  $t_2$  are determined as shown in the figure 2.7. The points used as referenced is kept as constant for all measuring data with regards to COR for all cases and simulations in this study. Thus, the following parameters are found using the above determined parameters.

Time between the successive step time after impact is given by,

$$t = t_2 - t_1 \quad (2.5)$$

Distance between the reference nodes is given by

$$d = d_2 - d_1 \quad (2.6)$$

Output velocity of the shots after impact is given by

$$V_{out} = d/t \quad (2.7)$$

Input velocity is determined from normal velocity and angle of impact (case 1 simulations) or given as an input to the simulation and kept constant (case 2).

Therefore, restitution coefficient is given by,

$$COR = V_{out} / V_{in} \quad (2.8)$$

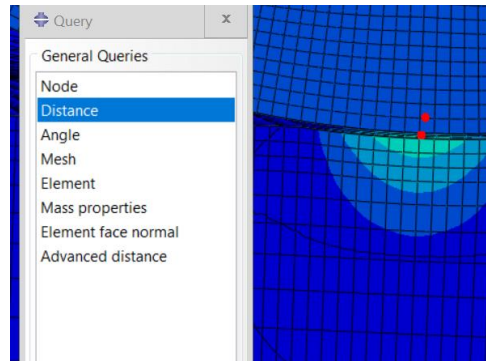
Considering the decomposition of the velocity vector,

$$COR_x = V_{x\_out} / V_{x\_in} \quad (2.9)$$

$$COR_y = V_{y\_out} / V_{y\_in} \quad (2.10)$$

This helps in determining the COR in both the direction and infer how COR differs with respect to change in velocity and change in the angle of impact.

The distance between these two nodes is calculated in successive step time after impact as shown in figure 2.8 and thus providing output velocity of the shot and COR.



(a)

Select the first node for the distance calculation TARGET-1 56705				
Scale:	1.00000e+00,	1.00000e+00,	1.00000e+00,	-
Deformed distance (unscaled):	7.37681e-02,	-1.33514e-02,	-1.33696e-04,	7.49668e-02
Deformed distance (scaled):	7.37681e-02,	-1.33514e-02,	-1.33696e-04,	7.49668e-02
Relative displacement (unscaled):	4.94977e-04,	-6.33250e-03,	-1.33734e-04,	6.35323e-03

(b)

Figure 2.8 A graphical representation of measuring distance between the nodes

The data collected has the information regarding the distance moved in x and y direction and thus aids in computing COR also in x and y direction.

## 2.2.6 Post Processing

Once the simulation is done for varying cases of orientation angle, the results are analysed as following.

Once the simulation is executed, the COR is determined as mentioned in section 2.2.4 and 2.2.5. After the impact, target surface gets deformed. The data regarding the deformations are collected and exported to MATLAB where the data is plotted as graph. The diameter of dimple and height of the dimple are calculated for all the simulations in each case. The changes in these evaluation parameters with respect to change in impact orientation and impact velocity is recorded and studied.

A path is created along the central cross section of the target after impact and variation in surface along U2 direction is studied to determine the depth and diameter of the dimple. Deformation along the path as shown in the figure 2.9 is recorded and parameters such as depth of the dimple and diameter of the dimple are determined for all the simulations in each case in this study.

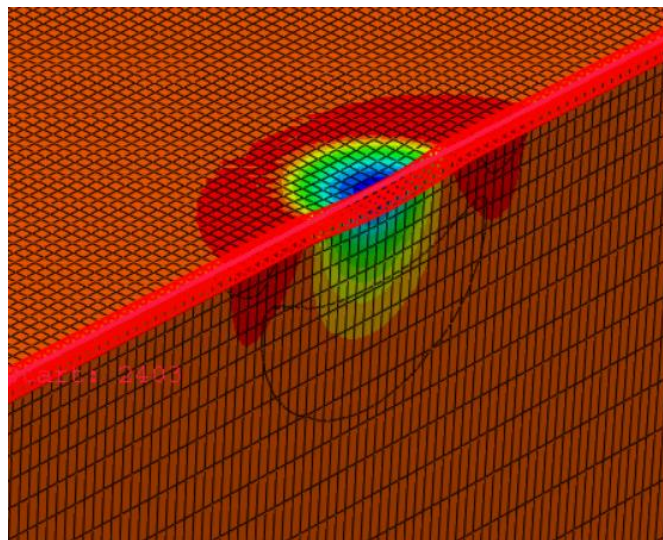


Figure 2.9 A generic representation of path created to plot dimple diameter and dimple height

## Chapter 3

# Results and Discussions

### 3.1 Results for simulations of case 1

For the first case, the normal velocity is kept constant but the 2 D velocity is changed. Normal velocity denotes the velocity in y direction in this study. It denotes the direction perpendicular to the top surface of the target substrate. While the 2D velocity and velocity in x direction in this case changes with respect to the changes in the angle of impact as explained in section 2.2.3.1. and it is determined as said in that section.

The following table depicts various simulations studied under case 1 in this study.

Angle (XY plane)	$V_x$ (mm/s)	$V_y$ (mm/s)	Velocity, $V$ (mm/s)
90	0	-3600	3600
75	964.6170928	-3600	3726.994249
60	2078.460969	-3600	4156.921938
45	3600	-3600	5091.168825
30	6235.382907	-3600	7200
15	13435.38291	-3600	13909.3319

Table 3.1 variation in impact velocities wrt impact orientation with constant normal velocity

### 3.1.1 Simulation 1

Velocities along the 3 directions are set as shown in the figure below. The negative and positive sign are in correspondence to the direction modelled in the simulation.

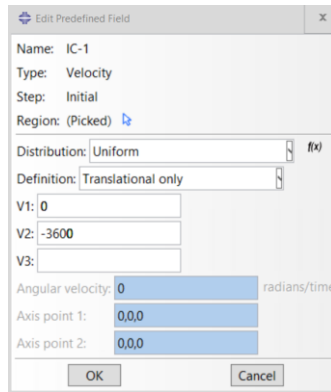


Figure 3.1 Velocities along different directions

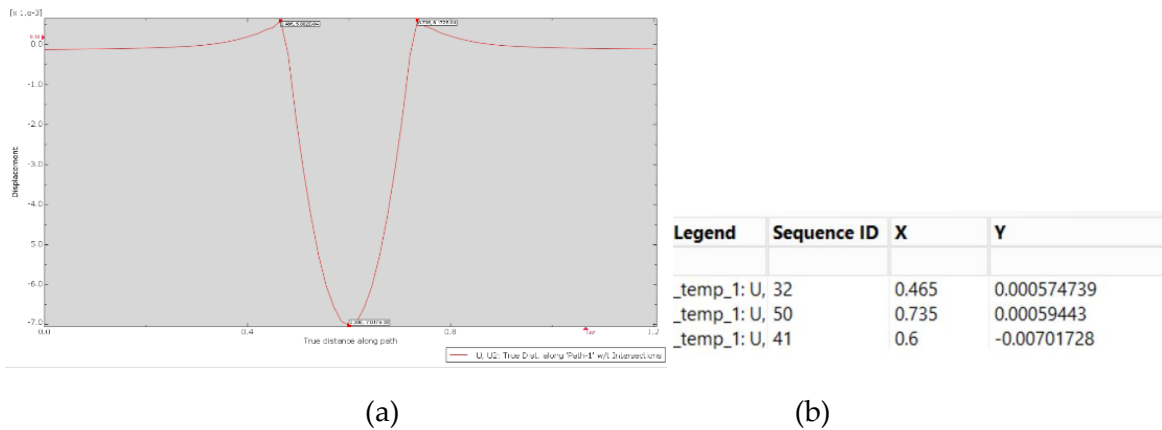


Figure 3.2 Dimple characteristics at 90-degree impact angle

Angle	Dimple Diameter	Dimple Depth
90	0.27 mm	0.008 mm

Table 3.2 Dimple characteristics

Parameter/ criterion	Angle	Input Velocity $V_{in}$	Distance $d_1$	Distance $d_2$	Distance moved $d$	Time taken $t$	Output velocity $V_{out}$	COR
Formulation / condition			At time ( $t_1$ ) $1 * e^{-05}$	At time ( $t_2$ ) $0.75e-06$	$d = d_2 - d_1$ (magnitude)	$t = t_2 - t_1$	$d/t$	$V_{out}/V_{in}$
units	degree	mm/s	mm	mm	mm	s	mm/s	
	90	0	0	0	0	0	-	-

Table 3.3 COR along x direction

Parameter/ criterion	Angle	Input Velocity $V_{in}$	Distance $d_1$	Distance $d_2$	Distance moved $d$	Time taken $t$	Output velocity $V_{out}$	COR
Formulation / condition			At time ( $t_1$ ) $1 * e^{-05}$	At time ( $t_2$ ) $7e-06$	$d = d_2 - d_1$ (magnitude)	$t = t_2 - t_1$	$d/t$	$V_{out}/V_{in}$
units	degree	mm/s	mm	mm	mm	s	mm/s	
	90	3600	-0.0112	-0.0015	0.0097	3e-06	3233.33	0.898

Table 3.4 COR along y direction

Parameter/ criterion	Angle	Input Velocity $V_{in}$	Output velocity $V_{out}$	COR
Formulation / condition			$d/t$	$V_{out}/V_{in}$
units	degree	mm/s	mm/s	
	90	3600	3233.33	0.898

Table 3.5 COR wrt 2D Velocity

### 3.1.2 Simulation 2

Velocities along the 3 directions are set as shown in the figure 3.3.

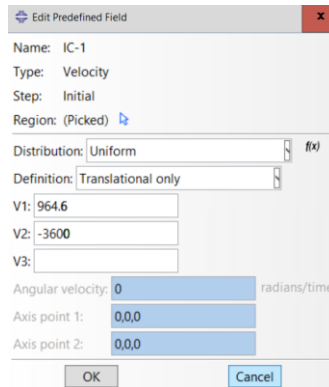
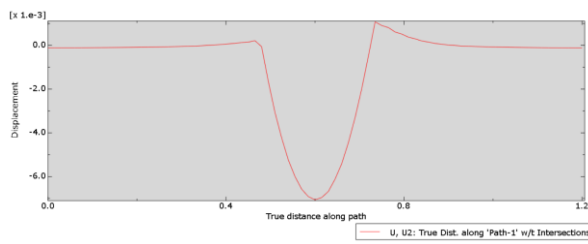


Figure 3.3 Velocities along different directions



(a)

_temp_1: U, 32	0.465	0.00021394
_temp_1: U, 50	0.735	0.00107383
_temp_1: U, 41	0.6	-0.00706053

(b)

Figure 3.4 Dimple characteristics at 75-degree impact angle

Angle	Dimple Diameter	Dimple Depth
75	0.25 mm	0.00706053 mm

Table 3.6 Dimple characteristics

Parameter/ criterion	Angle	Input Velocity $V_{in}$	Distance $d_1$	Distance $d_2$	Distance moved $d$	Time taken $t$	Output velocity $V_{out}$	COR
Formulation / condition			At time $(t_1)$ $1.3 \times 10^{-5}$	At time $(t_2)$ $1.3 \times 10^{-5}$	$d = d_2 - d_1$ (magnitude)	$t = t_2 - t_1$	$d/t$	$V_{out}/V_{in}$
units	degree	mm/s	mm	mm	mm	s	mm/s	
	75	964.6	0.00127	0.0008534	0.000417	$3 \times 10^{-6}$	138.9	0.144

Table 3.7 COR along x direction

Parameter/ criterion	Angle	Input Velocity $V_{in}$	Distance $d_1$	Distance $d_2$	Distance moved $D$	Time taken $t$	Output velocity $V_{out}$	COR
Formulation / condition			At time $(t_1)$ $1.3 \times 10^{-5}$	At time $(t_2)$ $1 \times 10^{-5}$	$d = d_2 - d_1$ (magnitude)	$t = t_2 - t_1$	$d/t$	$V_{out}/V_{in}$
units	degree	mm/s	mm	mm	mm	s	mm/s	
	75	3600	-0.0155	-0.0066	0.0089	$0.3 \times 10^{-5}$	2966.67	0.824

Table 3.8 COR along y direction

Parameter/ criterion	Angle	Input Velocity $V_{in}$	Output velocity $V_{out}$	COR
Formulation / condition			$d/t$	$V_{out}/V_{in}$
units	degree	mm/s	mm/s	
	75	3726.99	2969.9	0.79866

Table 3.9 COR wrt 2D Velocity

### 3.1.3 Simulation 3

Velocities along the 3 directions are set as shown in the figure below. The negative and positive sign are in correspondence to the direction modelled in the simulation. Dimple characteristics and corresponding data obtained during simulation is depicted in the figure 3.6.

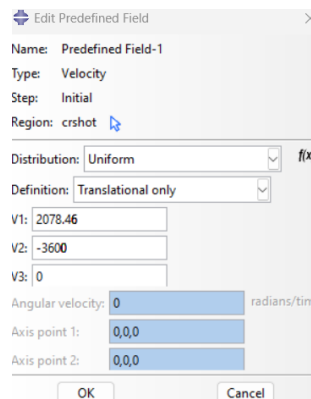
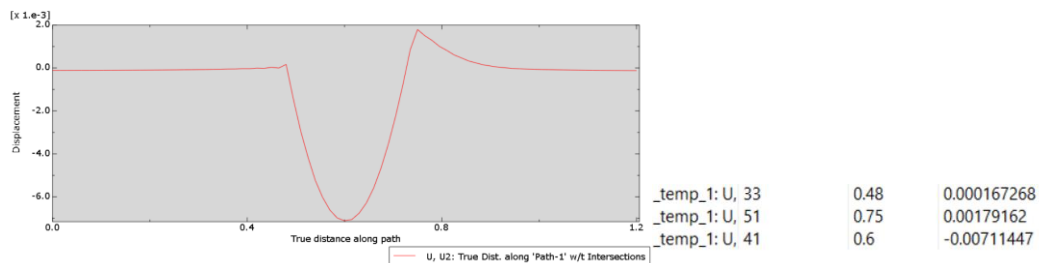


Figure 3.5 Velocities along different directions



(a)

(b)

Figure 3.6 Dimple characteristics at 60-degree impact angle

Angle	Dimple Diameter	Dimple Depth
60	0.25 mm	0.00711447 mm

Table 3.10 Dimple characteristics

Parameter/ criterion	Angle	Input Velocity $V_{in}$	Distance $d_1$	Distance $d_2$	Distance moved $d$	Time taken $t$	Output velocity $V_{out}$	COR
Formulation / condition			At time $(t_1)$ $1.3 \times 10^{-5}$	At time $(t_2)$ $1 \times 10^{-5}$	$d = d_2 - d_1$ (magnitude)	$t = t_2 - t_1$	$d/t$	$V_{out}/V_{in}$
units	degree	mm/s	mm	mm	mm	s	mm/s	
	60	2078.46	0.00201	0.000685	0.001325	$3 \times 10^{-6}$	441.67	0.2125

Table 3.11 COR along x direction

Parameter/ criterion	Angle	Input Velocity $V_{in}$	Distance $d_1$	Distance $d_2$	Distance moved $d$	Time taken $t$	Output velocity $V_{out}$	COR
Formulation / condition			At time $(t_1)$ $1.3 \times 10^{-5}$	At time $(t_2)$ $1 \times 10^{-5}$	$d = d_2 - d_1$ (magnitude)	$t = t_2 - t_1$	$d/t$	$V_{out}/V_{in}$
units	degree	mm/s	mm	mm	mm	s	mm/s	
	60	3600	-0.0131	-0.0044	0.0087	$3 \times 10^{-6}$	2900	0.815

Table 3.12 COR along y direction

Parameter/ criterion	Angle	Input Velocity $V_{in}$	Output velocity $V_{out}$	COR
Formulation / condition			$d/t$	$V_{out}/V_{in}$
units	degree	mm/s	mm/s	
	60	4156.92	2933.44	0.7056

Table 3.13 COR wrt 2D Velocity

### 3.1.4 Simulation 4

Velocities along the 3 directions are set as shown in the figure 3.7. The negative and positive sign are in correspondence to the direction modelled in the simulation.

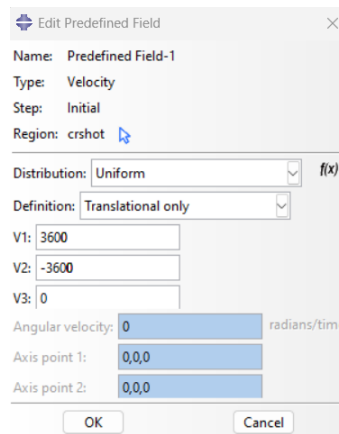


Figure 3.7 Velocities along different directions

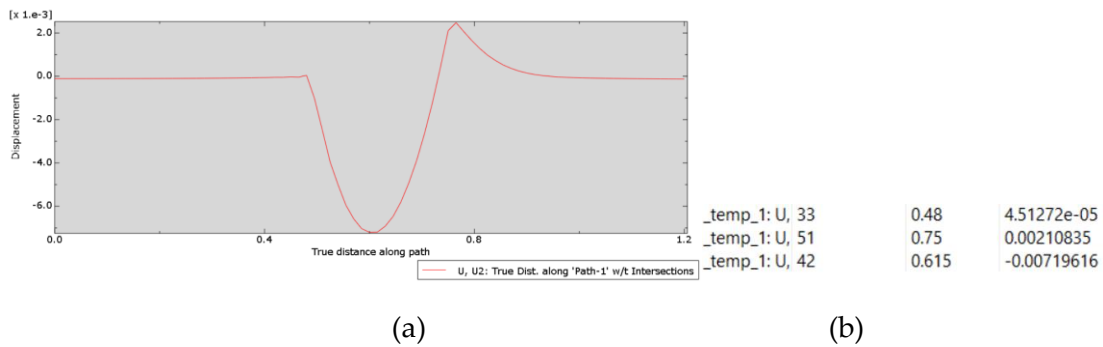


Figure 3.8 Dimple characteristics at 45-degree impact angle

Angle	Dimple Diameter	Dimple Depth
45	0.26 mm	0.007196 mm

Table 3.14 Dimple characteristics

Parameter/ criterion	Angle	Input Velocity $V_{in}$	Distance $d_1$	Distance $d_2$	Distance moved $d$	Time taken $t$	Output velocity $V_{out}$	COR
Formulation / condition			At time ( $t_1$ ) $1.3 \times 10^{-5}$	At time ( $t_2$ ) $1 \times 10^{-5}$	$d = d_2 - d_1$ (magnitude)	$t = t_2 - t_1$	$d/t$	$V_{out}/V_{in}$
units	degree	mm/s	mm	mm	mm	s	mm/s	
	45	3600	-0.0058	-0.0028	0.0038	$3 \times 10^{-6}$	1000	0.288

Table 3.15 COR along x direction

Parameter/ criterion	Angle	Input Velocity $V_{in}$	Distance $d_1$	Distance $d_2$	Distance moved $d$	Time taken $t$	Output velocity $V_{out}$	COR
Formulation / condition			At time ( $t_1$ ) $1.3 \times 10^{-5}$	At time ( $t_2$ ) $1 \times 10^{-5}$	$d = d_2 - d_1$ (magnitude)	$t = t_2 - t_1$	$d/t$	$V_{out}/V_{in}$
units	degree	mm/s	mm	mm	mm	s	mm/s	
	45	3600	-0.0141	-0.00554	0.00856	$3 \times 10^{-6}$	2853.33	0.793

Table 3.16 COR along y direction

Parameter/ criterion	Angle	Input Velocity $V_{in}$	Output velocity $V_{out}$	COR
Formulation / condition			$d/t$	$V_{out}/V_{in}$
units	degree	mm/s	mm/s	
	45	5091.9	3023.5	0.594

Table 3.17 COR wrt 2D Velocity

### 3.1.5 Simulation 5

Velocities along the 3 directions for the angle 30 degrees are set as shown in the figure below. The negative and positive sign are in correspondence to the direction modelled in the simulation.

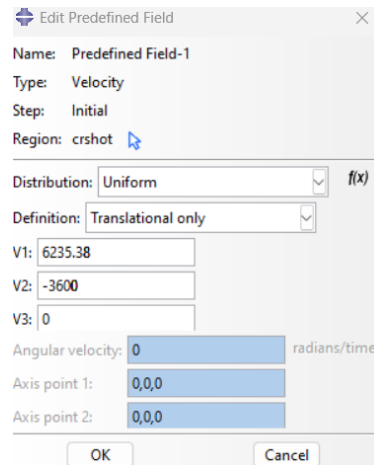


Figure 3.9 Velocities along different directions

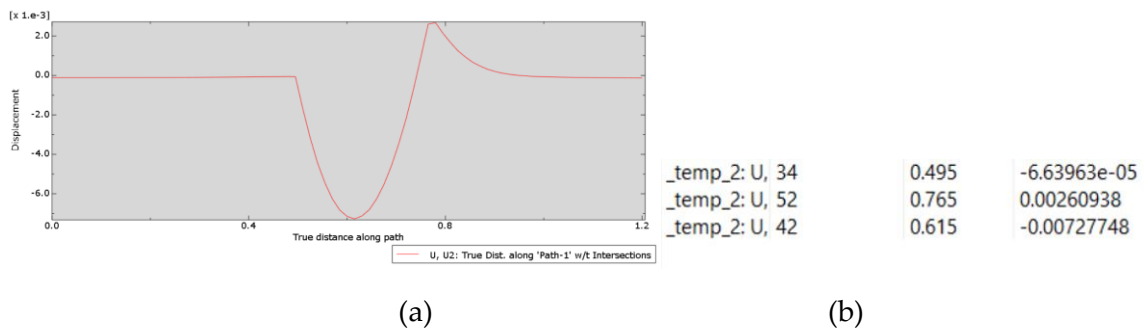


Figure 3.10 Dimple characteristics at 30-degree impact angle

Angle	Dimple Diameter	Dimple Depth
30	0.27 mm	0.007278 mm

Table 3.18 Dimple characteristics

Parameter/ criterion	Angle	Input Velocity $V_{in}$	Distance $d_1$	Distance $d_2$	Distance moved $d$	Time taken $t$	Output velocity $V_{out}$	COR
Formulation / condition			At time $(t_1)$ $1.3 \times 10^{-5}$	At time $(t_2)$ $1 \times 10^{-5}$	$d = d_2 - d_1$ (magnitude)	$t = t_2 - t_1$	$d/t$	$V_{out}/V_{in}$
units	degree	mm/s	mm	mm	mm	s	mm/s	
	30	6235.38	-0.0394	-0.03224	0.00716	$3 \times 10^{-6}$	2386.67	0.3828

Table 3.19 COR along x direction

Parameter/ criterion	Angle	Input Velocity $V_{in}$	Distance $d_1$	Distance $d_2$	Distance moved $d$	Time taken $t$	Output velocity $V_{out}$	COR
Formulation / condition			At time $(t_1)$ $1.3 \times 10^{-5}$	At time $(t_2)$ $1 \times 10^{-5}$	$d = d_2 - d_1$ (magnitude)	$t = t_2 - t_1$	$d/t$	$V_{out}/V_{in}$
units	degree	mm/s	mm	mm	mm	s	mm/s	
	30	3600	-0.0144	-0.00575	0.00865	$3 \times 10^{-6}$	2883.33	0.81

Table 3.20 COR along y direction

Parameter/ criterion	Angle	Input Velocity $V_{in}$	Output velocity $V_{out}$	COR
Formulation / condition			$d/t$	$V_{out}/V_{in}$
units	degree	mm/s	mm/s	
	30	7200	3742.97	0.52

Table 3.21 COR wrt 2D Velocity

### 3.1.6 Simulation 6

Velocities along the 3 directions for the angle 15 degrees are set as shown in the figure below. The negative and positive sign are in correspondence to the direction modelled in the simulation. Figure 3.12 depicts the dimple characteristics and corresponding data obtained from the simulation.

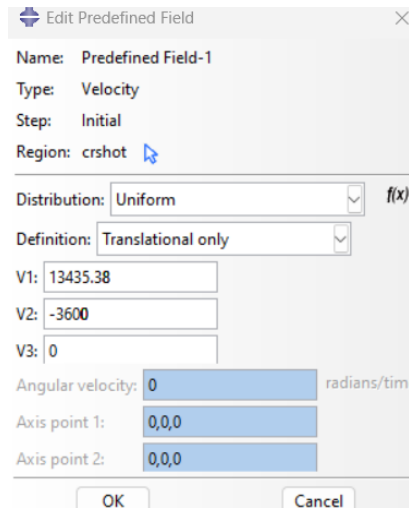


Figure 3.11 Velocities along different directions

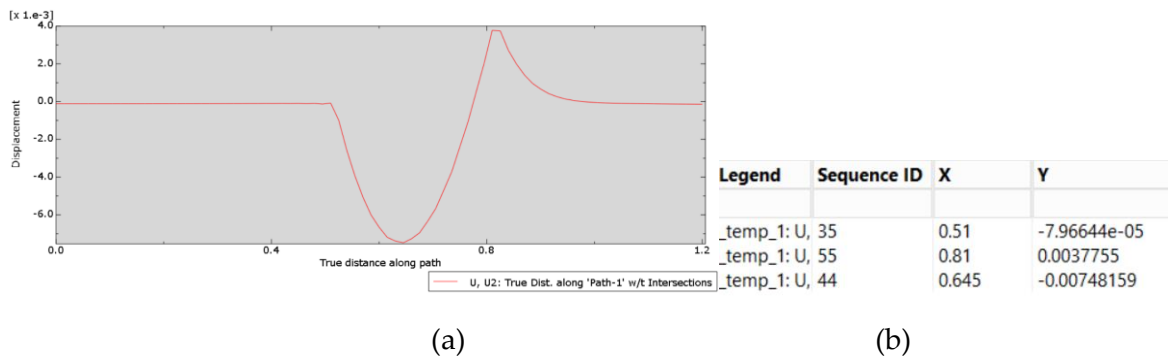


Figure 3.12 Dimple characteristics at 15-degree impact angle

Angle	Dimple Diameter	Dimple Depth
15	0.3 mm	0.0075 mm

Table 3.22 Dimple characteristics

Parameter/ criterion	Angle	Input Velocity $V_{in}$	Distance $d_1$	Distance $d_2$	Distance moved $d$	Time taken $t$	Output velocity $V_{out}$	COR
Formulation / condition			At time ( $t_1$ ) $1 \times 10^{-5}$	At time ( $t_2$ ) $0.75 \times 10^{-5}$	$d = d_2 - d_1$ (magnitude)	$t = t_2 - t_1$	$d/t$	$V_{out}/V_{in}$
units	degree	mm/s	mm	mm	mm	s	mm/s	
	15	13435.4	-0.1313	-0.1037	0.0276	$2.5 \times 10^{-6}$	11040	0.822

Table 3.23 COR along x direction

Parameter/ criterion	Angle	Input Velocity $V_{in}$	Distance $d_1$	Distance $d_2$	Distance moved $d$	Time taken $t$	Output velocity $V_{out}$	COR
Formulation / condition			At time ( $t_1$ ) $1 \times 10^{-5}$	At time ( $t_2$ ) $0.75 \times 10^{-5}$	$d = d_2 - d_1$ (magnitude)	$t = t_2 - t_1$	$d/t$	$V_{out}/V_{in}$
units	degree	mm/s	mm	mm	mm	s	mm/s	
	15	3600	-0.0158	-0.00876	0.00704	$2.5 \times 10^{-6}$	2816	0.782

Table 3.24 COR along y direction

Parameter/ criterion	Angle	Input Velocity $V_{in}$	Output velocity $V_{out}$	COR
Formulation / condition			$d/t$	$V_{out}/V_{in}$
units	degree	mm/s	mm/s	
	15	13909.3	11393.5	0.819

Table 3.25 COR wrt 2D Velocity

### 3.2 Results for simulations of case 2

For the second case, the 2D velocity is kept constant but the normal velocity is changed. Normal velocity denotes the velocity in y direction in this study. It denotes the direction perpendicular to the top surface of the target substrate. 2D Velocity is kept at 3600 mm/s. While the velocity in y direction and velocity in x direction in this case changes with respect to the changes in angle of impact as explained in section 2.2.3.1. and it is determined as said in that section.

The following table depicts various simulations studied under case 2 in this study.

Angle (XY plane)	V <sub>x</sub> (mm/s)	V <sub>y</sub> (mm/s)	Velocity (mm/s)
75	931.7485624	-3477.332975	3600
60	1800	-3117.691454	3600
45	2545.584412	-2545.584412	3600
30	3117.691454	-1800	3600
15	3477.332975	-931.7485624	3600

Table 3.26 variation in impact velocities wrt impact orientation with constant 2D velocity

### 3.2.1 Simulation 1

Velocities along the 3 directions are set as shown in the figure below. The negative and positive sign are in correspondence to the direction modelled in the simulation.

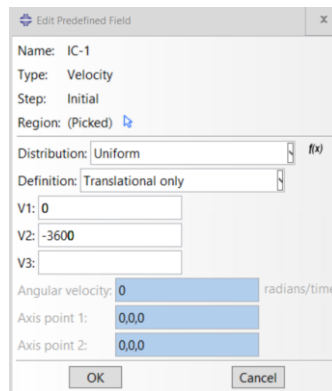
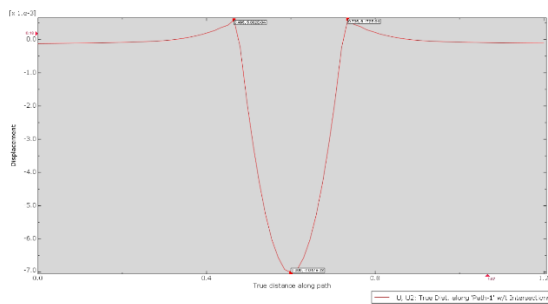


Figure 3.13 Velocities along different directions



Legend	Sequence ID	X	Y
_temp_1: U, 32		0.465	0.000574739
_temp_1: U, 50		0.735	0.00059443
_temp_1: U, 41		0.6	-0.00701728

(a)

(b)

Figure 3.14 Dimple characteristics at 90-degree impact angle

Angle	Dimple Diameter	Dimple Depth
90	0.27 mm	0.008 mm

Table 3.27 Dimple characteristics

Parameter/ criterion	Angle	Input Velocity $V_{in}$	Distance $d_1$	Distance $d_2$	Distance moved $d$	Time taken $t$	Output velocity $V_{out}$	COR
Formulation / condition			At time (t1) $1 \times 10^{-5}$	At time (t2) $0.75 \times 10^{-6}$	$d = d_2 - d_1$	$t = t_2 - t_1$	$d/t$	$V_{out}/V_{in}$
units	degree	mm/s	mm	mm	mm	s	mm/s	
	90	0	0	0	0	0	-	-

Table 3.28 COR along x direction

Parameter/ criterion	Angle	Input Velocity $V_{in}$	Distance $d_1$	Distance $d_2$	Distance moved $d$	Time taken $t$	Output velocity $V_{out}$	COR
Formulation / condition			At time (t1) $1 \times 10^{-5}$	At time (t2) $7 \times 10^{-6}$	$d = d_2 - d_1$ (magnitude)	$t = t_2 - t_1$	$d/t$	$V_{out}/V_{in}$
units	degree	mm/s	mm	mm	mm	s	mm/s	
	90	3600	-0.0112	-0.0015	0.0097	$3 \times 10^{-6}$	3233.33	0.898

Table 3.29 COR along y direction

Parameter/ criterion	Angle	Input Velocity $V_{in}$	Output velocity $V_{out}$	COR
Formulation / condition			$d/t$	$V_{out}/V_{in}$
units	degree	mm/s	mm/s	
	90	3600	3233.33	0.898

Table 3.30 COR wrt 2D Velocity

### 3.2.2 Simulation 2

Velocities along the 3 directions for 75-degree impact angle are set as shown in the figure below. The negative and positive sign are in correspondence to the direction modelled in the simulation.

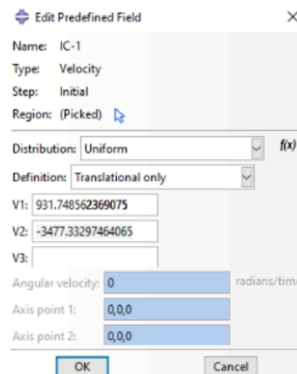
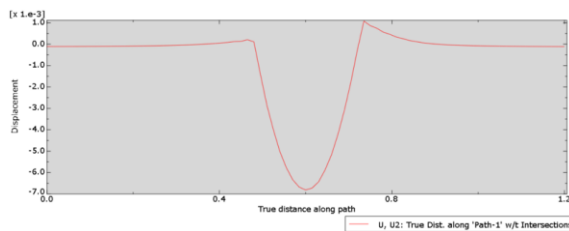


Figure 3.15 Velocities along different directions



(a)

Legend	Sequence ID	X	Y
_temp_1: U 33		0.482678	0.000536221
_temp_1: U 51		0.752677	0.000563893
_temp_1: U 42		0.617678	-0.00681453

(b)

Figure 3.16 Dimple characteristics at 75-degree impact angle

Angle	Dimple Diameter	Dimple Depth
75	0.269 mm	0.00736 mm

Table 3.31 Dimple characteristics

Parameter/ criterion	Angle	Input Velocity $V_{in}$	Distance $d_1$	Distance $d_2$	Distance moved $d$	Time taken $t$	Output velocity $V_{out}$	COR
Formulation / condition			At time $(t_1)$ $1 \times 10^{-5}$	At time $(t_2)$ $7.5 \times 10^{-6}$	$d = d_2 - d_1$ (magnitude)	$t = t_2 - t_1$	$d/t$	$V_{out}/V_{in}$
units	degree	mm/s	mm	mm	mm	s	mm/s	
	75	931.7485	$3.99 \times 10^{-4}$	-0.0004	$8 \times 10^{-4}$	$2.5 \times 10^{-6}$	320	0.35

Table 3.32 COR along x direction

Parameter/ criterion	Angle	Input Velocity $V_{in}$	Distance $d_1$	Distance $d_2$	Distance moved $d$	Time taken $t$	Output velocity $V_{out}$	COR
Formulation / condition			At time $(t_1)$ $1 \times 10^{-5}$	At time $(t_2)$ $7.5 \times 10^{-6}$	$d = d_2 - d_1$ (magnitude)	$t = t_2 - t_1$	$d/t$	$V_{out}/V_{in}$
units	degree	mm/s	mm	mm	mm	s	mm/s	
	75	3477.33	-0.00653	0.00115	$7.68 \times 10^{-3}$	$2.5 \times 10^{-6}$	3072	0.884

Table 3.33 COR along y direction

Parameter/ criterion	Angle	Input Velocity $V_{in}$	Output velocity $V_{out}$	COR
Formulation / condition			$d/t$	$V_{out}/V_{in}$
units	degree	mm/s	mm/s	
	75	3600	3088.62	0.858

Table 3.34 COR wrt 2D Velocity

### 3.2.3 Simulation 3

Velocities along the 3 directions for 60 degrees impact angle are set as shown in the figure below. The negative and positive sign are in correspondence to the direction modelled in the simulation.

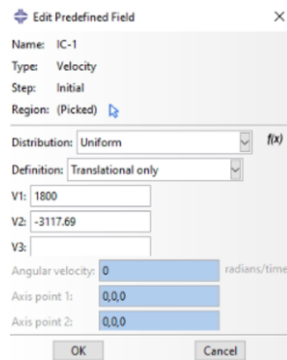


Figure 3.17 Velocities along different directions

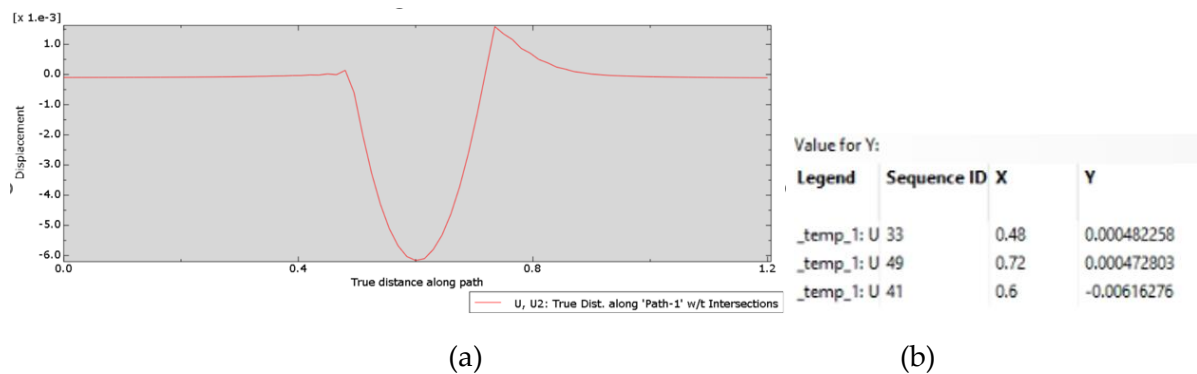


Figure 3.18 Dimple characteristics at 60-degree impact angle

Angle	Dimple Diameter	Dimple Depth
60	0.24 mm	0.00667 mm

Table 3.35 Dimple characteristics

Parameter/ criterion	Angle	Input Velocity $V_{in}$	Distance $d_1$	Distance $d_2$	Distance moved $d$	Time taken $t$	Output velocity $V_{out}$	COR
Formulation / condition			At time $(t_1)$ $1 \times 10^{-5}$	At time $(t_2)$ $0.75 \times 10^{-5}$	$d = d_2 - d_1$ (magnitude)	$t = t_2 - t_1$	$d/t$	$V_{out}/V_{in}$
units	degree	mm/s	mm	Mm	mm	s	mm/s	
	60	1800	0.000399	-0.0004	0.0008	$2.5 \times 10^{-6}$	390	0.212

Table 3.36 COR along x direction

Parameter/ criterion	Angle	Input Velocity $V_{in}$	Distance $d_1$	Distance $d_2$	Distance moved $d$	Time taken $t$	Output velocity $V_{out}$	COR
Formulation / condition			At time $(t_1)$ $1 \times 10^{-5}$	At time $(t_2)$ $0.75 \times 10^{-5}$	$d = d_2 - d_1$ (magnitude)	$t = t_2 - t_1$	$d/t$	$V_{out}/V_{in}$
units	degree	mm/s	mm	mm	mm	s	mm/s	
	60	3117.69	-0.00633	-0.00036	$6.68 \times 10^{-3}$	$2.5 \times 10^{-6}$	2674.97	0.858

Table 3.37 COR along y direction

Parameter/ criterion	Angle	Input Velocity $V_{in}$	Output velocity $V_{out}$	COR
Formulation / condition			$d/t$	$V_{out}/V_{in}$
units	degree	mm/s	mm/s	
	60	3600	2703.25	0.751

Table 3.38 COR wrt 2D Velocity

### 3.2.4 Simulation 4

Velocities along the 3 directions for 45 degrees impact angle are set as shown in the figure below. The negative and positive sign are in correspondence to the direction modelled in the simulation.

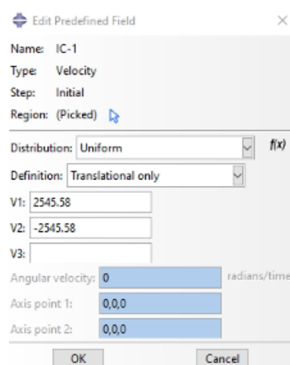


Figure 3.19 Velocities along different directions

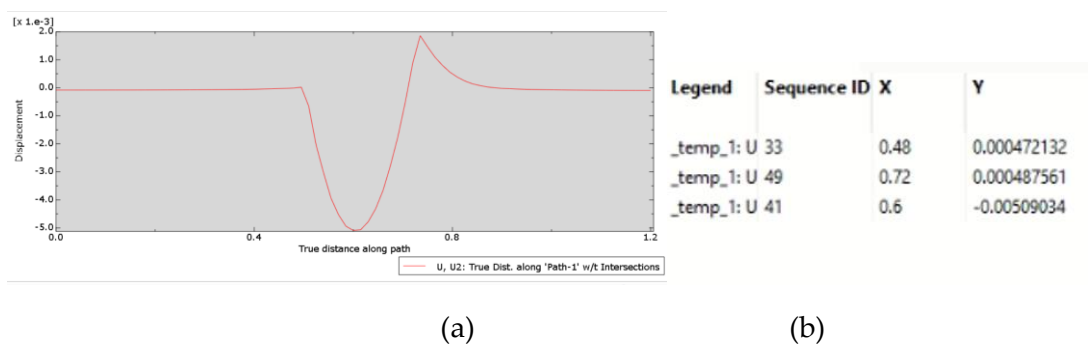


Figure 3.20 Dimple characteristics at 45-degree impact angle

Angle	Dimple Diameter	Dimple Depth
45	0.24 mm	0.00557 mm

Table 3.39 Dimple characteristics

Parameter/ criterion	Angle	Input Velocity $V_{in}$	Distance $d_1$	Distance $d_2$	Distance moved $d$	Time taken $t$	Output velocity $V_{out}$	COR
Formulation / condition			At time $(t_1)$ $1 \times 10^{-5}$	At time $(t_2)$ $0.75 \times 10^{-5}$	$d = d_2 - d_1$ (magnitude)	$t = t_2 - t_1$	$d/t$	$V_{out}/V_{in}$
units	degree	mm/s	mm	mm	mm	s	mm/s	
	45	2545.58	-0.005	-0.0025	$2.46 \times 10^{-3}$	$2.5 \times 10^{-6}$	982.1	0.386

Table 3.40 COR along x direction

Parameter/ criterion	Angle	Input Velocity $V_{in}$	Distance $d_1$	Distance $d_2$	Distance moved $d$	Time taken $t$	Output velocity $V_{out}$	COR
Formulation / condition			At time $(t_1)$ $1 \times 10^{-5}$	At time $(t_2)$ $7.5 \times 10^{-6}$	$d = d_2 - d_1$ (magnitude)	$t = t_2 - t_1$	$d/t$	$V_{out}/V_{in}$
units	degree	mm/s	mm	mm	mm	s	mm/s	
	45	2545.58	-0.0053	0.0003	$5.33 \times 10^{-3}$	$2.5 \times 10^{-6}$	2120.46	0.833

Table 3.41 COR along y direction

Parameter/ criterion	Angle	Input Velocity $V_{in}$	Output velocity $V_{out}$	COR
Formulation / condition			$d/t$	$V_{out}/V_{in}$
units	degree	mm/s	mm/s	
	45	3600	2336.9	0.649

Table 3.42 COR wrt 2D Velocity

### 3.2.5 Simulation 5

Velocities along the 3 directions for 30-degree impact angle are set as shown in the figure below. The negative and positive sign are in correspondence to the direction modelled in the simulation.

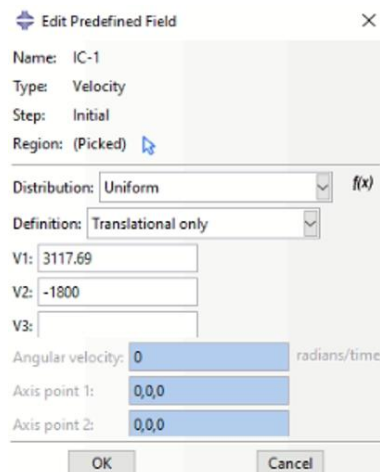


Figure 3.21 Velocities along different directions

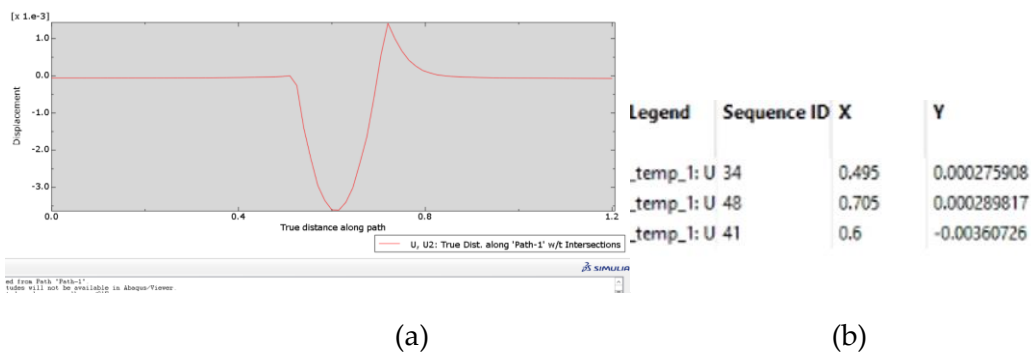


Figure 3.22 Dimple characteristics at 30-degree impact angle

Angle	Dimple Diameter	Dimple Depth
30	0.21 mm	0.00389 mm

Table 3.43 Dimple characteristics

Parameter/ criterion	Angle	Input Velocity $V_{in}$	Distance $d_1$	Distance $d_2$	Distance moved $d$	Time taken $t$	Output velocity $V_{out}$	COR
Formulation / condition			At time ( $t_1$ ) $1 \times 10^{-5}$	At time ( $t_2$ ) $0.75 \times 10^{-5}$	$d = d_2 - d_1$ (magnitude)	$t = t_2 - t_1$	$d/t$	$V_{out}/V_{in}$
units	degree	mm/s	mm	mm	mm	s	mm/s	
	30	3117.7	-1.68e-2	-1.39e-2	2.9e-3	2.5e-6	1160	0.37

Table 3.44 COR along x direction

Parameter/ criterion	Angle	Input Velocity $V_{in}$	Distance $d_1$	Distance $d_2$	Distance moved $d$	Time taken $t$	Output velocity $V_{out}$	COR
Formulation / condition			At time ( $t_1$ ) $1 \times 10^{-5}$	At time ( $t_2$ ) $0.75 \times 10^{-5}$	$d = d_2 - d_1$ (magnitude)	$t = t_2 - t_1$	$d/t$	$V_{out}/V_{in}$
units	degree	mm/s	mm	mm	mm	s	mm/s	
	30	1800	0.00322	4.93e-4	3.71e-3	2.5e-6	1485	0.825

Table 3.45 COR along y direction

Parameter/ criterion	Angle	Input Velocity $V_{in}$	Output velocity $V_{out}$	COR
Formulation / condition			$d/t$	$V_{out}/V_{in}$
units	degree	mm/s	mm/s	
	30	3600	1884.36	0.53

Table 3.46 COR wrt 2D Velocity

### 3.2.6 Simulation 6

Velocities along the 3 directions for 15-degree impact angle are set as shown in the figure below. The negative and positive sign are in correspondence to the direction modelled in the simulation.

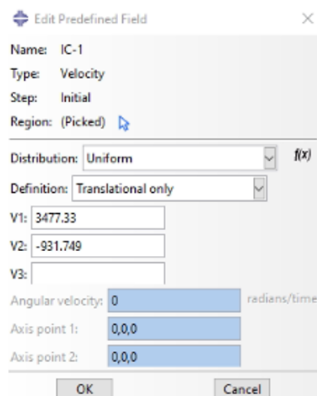


Figure 3.23 Velocities along different directions

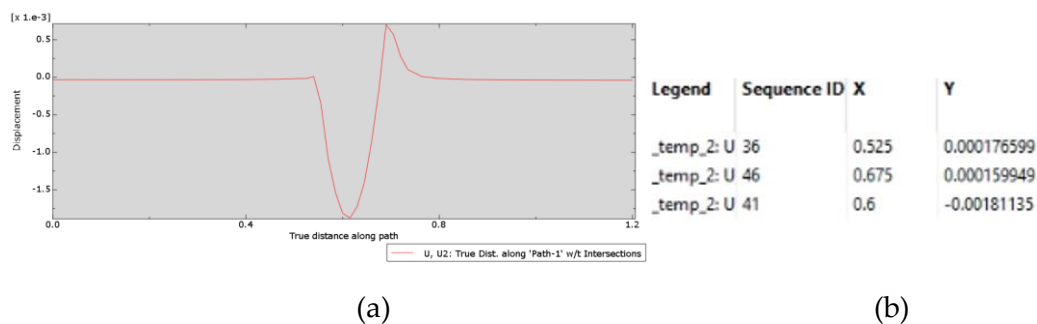


Figure 3.24 Dimple characteristics at 15-degree impact angle

Angle	Dimple Diameter	Dimple Depth
15	0.15 mm	0.00198 mm

Table 3.47 Dimple characteristics

Parameter/ criterion	Angle	Input Velocity $V_{in}$	Distance $d_1$	Distance $d_2$	Distance moved $d$	Time taken $t$	Output velocity $V_{out}$	COR
Formulation / condition			At time ( $t_1$ ) $1 \times 10^{-5}$	At time ( $t_2$ ) $0.75 \times 10^{-5}$	$d = d_2 - d_1$ (magnitude)	$t = t_2 - t_1$	$d/t$	$V_{out}/V_{in}$
units	degree	mm/s	mm	mm	mm	s	mm/s	
	15	3477.33	$7.3 \times 10^{-2}$	$0. \times 10^{-3}$	$7.2 \times 10^{-2}$	$2.5 \times 10^6$	292	0.31

Table 3.48 COR along x direction

Parameter/ criterion	Angle	Input Velocity $V_{in}$	Distance $d_1$	Distance $d_2$	Distance moved $d$	Time taken $t$	Output velocity $V_{out}$	COR
Formulation / condition			At time ( $t_1$ ) $1 \times 10^{-5}$	At time ( $t_2$ ) $0.75 \times 10^{-5}$	$d = d_2 - d_1$ (magnitude)	$t = t_2 - t_1$	$d/t$	$V_{out}/V_{in}$
units	degree	mm/s	mm	mm	mm	s	mm/s	
	15	931.75	$7.02 \times 10^{-3}$	$0.1 \times 10^{-4}$	$7 \times 10^{-3}$	$2.5 \times 10^{-6}$	2810	0.81

Table 3.49 COR along y direction

Parameter/ criterion	Angle	Input Velocity $V_{in}$	Output velocity $V_{out}$	COR
Formulation / condition			$d/t$	$V_{out}/V_{in}$
units	degree	mm/s	mm/s	
	15	3600	2823.1	0.784

Table 3.50 COR wrt 2D Velocity

## 3.3 Discussion on results

### 3.3.1 Dimple Characteristics

Under case 1 simulations, the normal velocity is fixed at 3600 mm/s. The velocity along the x direction changes in accordance to the change in the angle of impact. Owing to variation in Velocity fields, the total 2D Velocity change with respect to impact angle. It can be inferred from the results that variation in depth of indentation is not much. This is because the penetration depth depends on the normal velocity (y direction) and since it is constant, the depth is unaffected.

However, increase in tangential velocity (x direction in this case) affects the diameter of the dimple rather than the depth. It could be inferred from the figure 3.25 given below that the diameter of dimple is altered (increased) with increase in velocity in x direction.

In other words, decrease in angle of impact leads to increased tangential velocity when the normal velocity is constant.

Therefore, under such circumstances, dimple diameter increases with decrease in angle of impact and dimple depth is unaltered owing to constant normal velocity. This can be inferred in the figure 3.25 where we could find that dimple diameter increases with increases in impact angle and increase in tangential velocity with constant normal velocity.

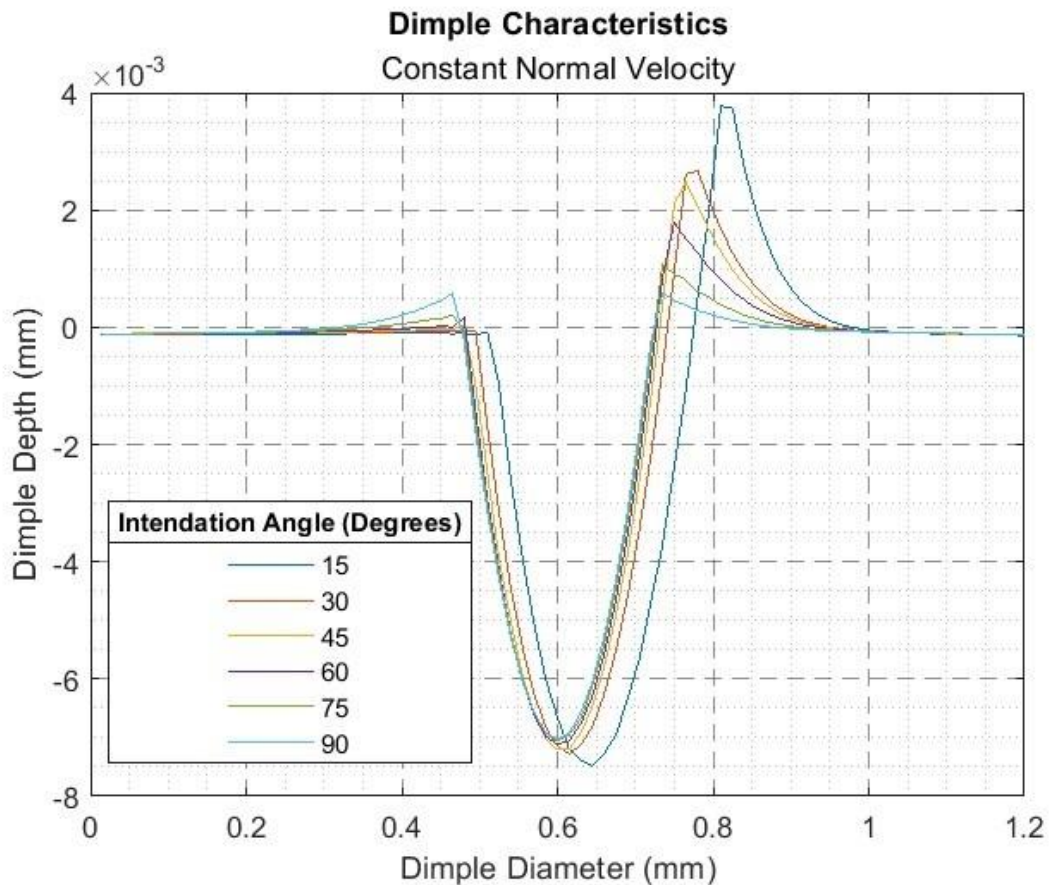


Figure 3.25 Dimple morphology owing to different simulations under case 1

Under case 2 simulations, total 2D velocity is fixed constant at 3600 mm/s. Therefore, the velocity in x and y direction changes with respect to changes in angle of impact. From the figure 3.26 given below, it could be inferred that the dimple depth increased with respect to increase angle of impact.

At lower angle of impact, velocity component in x direction is higher and therefore the tangential velocity is higher and at higher impact angles, velocity component in y direction is higher and therefore, normal velocity is higher.

Under given circumstances, decrease in angle of impact decreases the normal velocity of the shot. This reduces the depth of the dimple. Since the total 2D velocity is constant, the change in velocity components with respect to change in angle of impact, affects the dimple depth and dimple diameter.

Dimple diameter and dimple depth decreases with respect to reduction in angle of impact. This can be inferred in the figure 3.26 where we could find that dimple diameter decreases with decrease in impact angle and increase in the tangential velocity. Decrease in normal velocity results in decrease in depth of the impact with respect to decrease in angle of impact.

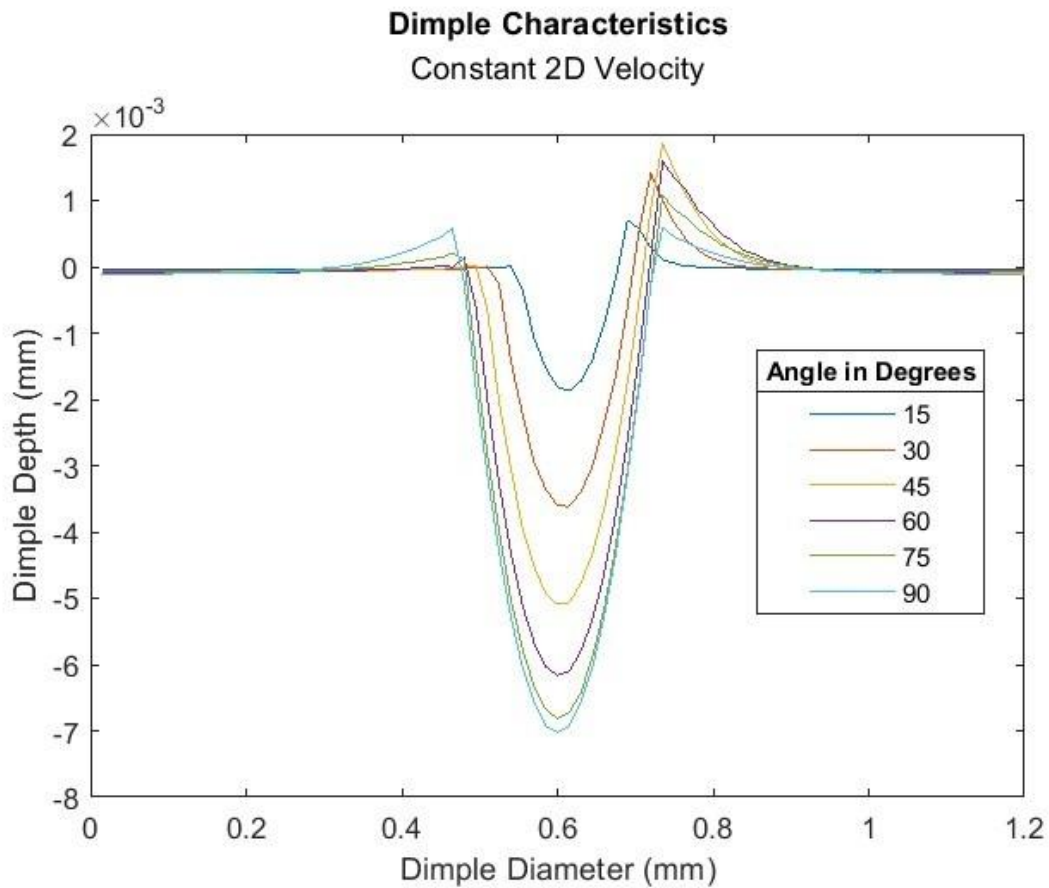


Figure 3.26 Dimple morphology owing to different simulations under case 2

### 3.3.2 Variation of COR

Considering the first case, where the normal velocity is maintained constant at 3600 mm/s, COR decreases along the y direction when the impact angle is reduced. This is because whenever the angle of impact decreases the energy lost during the collision between the bodies increases. On the contrary decrease in angle of impact tends to increase COR in x direction as depicted in the figure 3.27.

When the impact angle decreases, motion of shot becomes oblique rather than being perpendicular and therefore, the energy transferred in x direction is higher. But in this case velocity in y direction is at constant and therefore the reduction of COR in y direction is not much as seen in the figure 3.27 and it is above 0.78 which exhibits a better elastic collision between the shot and the target surface.

Similarly, due to this oblique angle of impact, most of the collision energy goes into x direction rather than into compressing and rebounding in y direction. In addition to it, the velocity in x direction increases with each case under first simulation. This makes the COR in x direction increase as shown in figure 3.27.

This results in decrease in COR with respect to decrease in angle of impact as more energy is lost during collision and the kinetic energy of the shot is not conserved. In addition to these criteria, friction between the shot and target surface can also lead to loss in kinetic energy of the shot and reduction in COR.

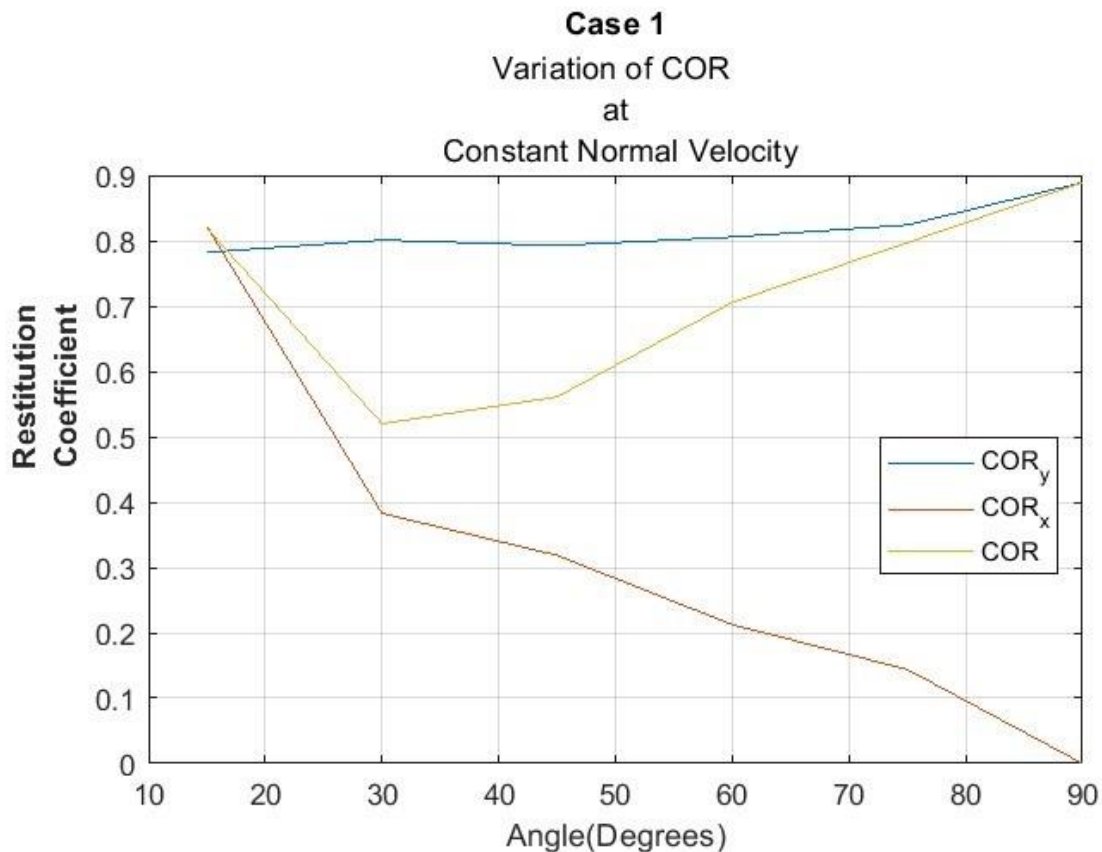


Figure 3.27 variation of COR under case 1

In the second case, the total 2D Velocity is maintained constant at 3600 mm/s. Thus, when the angle of impact is 90 degrees, the velocity component in x direction is zero and impact is in perpendicular direction to the target surface. After impact some energy is lost due to friction between the shot and target surface.

As the angle of impact decreases, the velocity in x direction increase at expense of velocity in y direction and therefore most of the energy goes into the x direction which is parallel to the surface. This results in decreased activity of compression by shots.

The decrease in velocity in normal direction with respect to constant 2D Velocity and decrease in impact angle, leads to decreased energy in y direction. Therefore, the COR in y direction decreases at the expense of increase in velocity in x direction.

Even though, there is a decrease in COR in y direction, the reduction is very small and COR remains in the range above 0.82, thus exhibiting better elastic collision between the shot and the target surface. Figure 3.28 depicts the decrease in COR with respect to decrease in angle of impact.

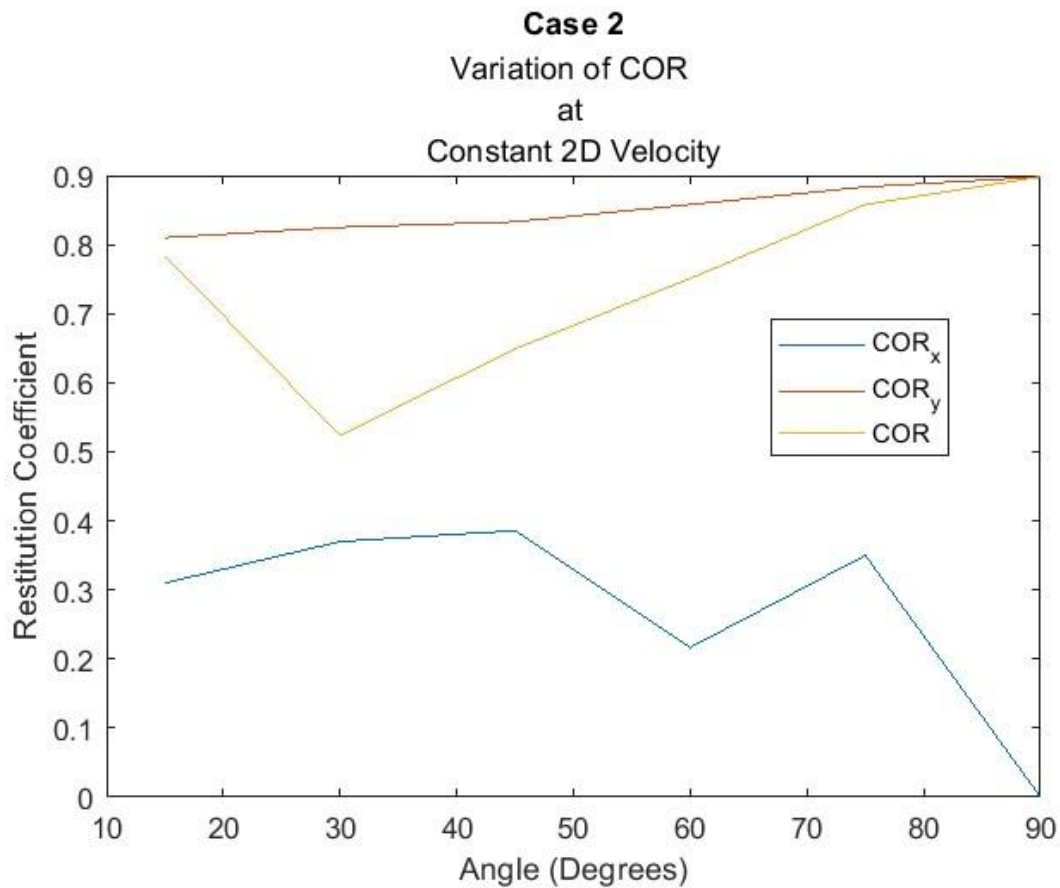


Figure 3.28 variation of COR under case 2

## Chapter 4

### Conclusions

The motivation behind this thesis is to build a numerical model that would act like an interface for the simulation of Ultrasonic shot peening considering a single impact that aids in understanding influence of various impact angle orientation and impact velocity on the dimple created.

The main objectives of the thesis are to develop a model that uses material and process parameters as inputs and helps in determining surface morphology by providing Dimple height, Dimple Diameter as output along with restitution coefficient which helps in determining amount of energy transferred during each impact at different impact orientation. The model is built for a particular material 316L stainless steel impinged by 100Cr6 shot. The dimple characteristics with respect to change in impact angle and corresponding change in impact velocity are studied. The model provided is established for angles 0, 15, 30, 45, 60, 75, 90 degrees respectively with corresponding changes in impact velocities. The model provided in the study can later be extrapolated for multiple impacts and for different materials for the future studies.

In this study, a numerical model is built which considers several parameters of the USP Process such as material property of the shot and material properties of target which includes the plasticity model for determining plastic properties of the target material.

It also takes into account the parameters like shot velocity, impact orientation and aids in post processing by determining evaluation parameters like dimple height, dimple width and restitution coefficient.

The drawing conclusions can be listed as followed:

1. Influence of impact angle over penetration effects on target material is studied. In addition to it, influence of change in impact velocity over such effects are studied.
2. Variations in restitution coefficient with respect to different angle of impact and different impact velocity are studied along various directions.

The model is built for a particular material (316L stainless steel) and therefore influence of such process parameters (impact angle) over evaluation parameter (dimple characteristics) for different materials can be a possible study. Another promising study would be incorporating suitable multiple impact model.

# Bibliography

- [1] Chaise, T., Li, J., Nélias, D., Kubler, R., Taheri, S., Douchet, G., Robin, V., & Gilles, P. (2012). Modelling of multiple impacts for the prediction of distortions and residual stresses induced by ultrasonic shot peening (USP). *Journal of Materials Processing Technology*, 212(10), 2080–2090.  
<https://doi.org/10.1016/j.jmatprotec.2012.05.005>
- [2] Tao, N. R., Sui, M. L., Lu, J., & Lu, K. (1999). SURFACE NANOCRYSTALLIZATION OF IRON INDUCED BY ULTRASONIC SHOT PEENING.
- [3] Wu, X., Tao, N., Hong, Y., Xu, B., Lu, J., & Lu, K. (2002). Microstructure and evolution of mechanically-induced ultrafine grain in surface layer of AL-alloy subjected to USSP. In *Acta Materialia* (Vol. 50). [www.actamat-journals.com](http://www.actamat-journals.com)
- [4] Yin, F., Hua, L., Wang, X., Rakita, M., & Han, Q. (2014). Numerical modelling and experimental approach for surface morphology evaluation during ultrasonic shot peening. *Computational Materials Science*, 92, 28–35.  
<https://doi.org/10.1016/j.commatsci.2014.05.011>
- [5] Li, Y., Chen, J., Luo, Y., Zhao, S., & Wang, L. (2023). Strain rate and orientation dependence of deformation behavior in a single crystal superalloy subjected to ultrasonic shot peening. *Vacuum*, 209. <https://doi.org/10.1016/j.vacuum.2022.111801>
- [6] Guagliano, M., Bagherifard, S., & Sarabi, B. (2016). POLITECNICO DI MILANO (LECCO CAMPUS) DESIGN OF ULTRASONIC SHOT PEENING DEVICE.
- [7] Li, P., Hu, S., Liu, Y., Hua, L., & Yin, F. (2022). Surface Nanocrystallization and Numerical Modeling of 316L Stainless Steel during Ultrasonic Shot Peening Process. *Metals*, 12(10). <https://doi.org/10.3390/met12101673>
- [8] Wu, X., Tao, N., Hong, Y., Xu, B., Lu, J., & Lu, K. (2002). Microstructure and evolution of mechanically-induced ultrafine grain in surface layer of AL-alloy subjected to USSP. In *Acta Materialia* (Vol. 50). [www.actamat-journals.com](http://www.actamat-journals.com)

- [9] Champaigne, J. (n.d.). *Shot Peening Overview*. <http://www.shotpeener.com>
- [10] Ganguly, S., Chaubey, A. K., Sahoo, R., Kushwaha, A., Basu, A., Majhi, J., & Gupta, M. (2023). Influence of ultrasonic shot peening on the microstructure and impression creep performance of squeeze-cast AZ91 alloy reinforced with graphene nanoplatelets. *Journal of Alloys and Compounds*, 938. <https://doi.org/10.1016/j.jallcom.2022.168640>
- [11] Li, P., Hu, S., Liu, Y., Hua, L., & Yin, F. (2022). Surface Nanocrystallization and Numerical Modeling of 316L Stainless Steel during Ultrasonic Shot Peening Process. *Metals*, 12(10). <https://doi.org/10.3390/met12101673>
- [12] Rakita, M., Wang, M., Han, Q., Liu, Y., & Yin, F. (2013). Ultrasonic shot peening. *International Journal of Computational Materials Science and Surface Engineering*, 5(3), 189. <https://doi.org/10.1504/ijcmsse.2013.056948>
- [13] Bagheri, S., & Guagliano, M. (2009). Review of shot peening processes to obtain nanocrystalline surfaces in metal alloys. In *Surface Engineering* (Vol. 25, Issue 1, pp. 3–14). <https://doi.org/10.1179/026708408X334087>
- [14] Wang, C., Liu, X., Song, Q., Tian, K., Fei, S., Deng, H., & Shen, G. (2024). Effects of ultrasonic shot peening followed by surface mechanical rolling on mechanical properties and fatigue performance of 2024 aluminum alloy. *Engineering Fracture Mechanics*, 311. <https://doi.org/10.1016/j.engfracmech.2024.110538>
- [15] Badreddine, J., Rouhaud, E., Micoulaut, M., & Remy, S. (2014). Simulation of shot dynamics for ultrasonic shot peening: Effects of process parameters. *International Journal of Mechanical Sciences*, 82, 179–190. <https://doi.org/10.1016/j.ijmecsci.2014.03.006>
- [16] Rakita, M., Wang, M., Han, Q., Liu, Y., & Yin, F. (2013). Ultrasonic shot peening. *International Journal of Computational Materials Science and Surface Engineering*, 5(3), 189. <https://doi.org/10.1504/ijcmsse.2013.056948>
- [17] Guagliano, M. (n.d.). *Relating Almen intensity to residual stresses induced by shot peening: a numerical approach*.

- [18] Frija, M., Hassine, T., Fathallah, R., Bouraoui, C., & Dogui, A. (2006). Finite element modelling of shot peening process: Prediction of the compressive residual stresses, the plastic deformations and the surface integrity. *Materials Science and Engineering: A*, 426(1–2), 173–180. <https://doi.org/10.1016/j.msea.2006.03.097>
- [19] Hong, T., Ooi, J. Y., & Shaw, B. (2008). A numerical simulation to relate the shot peening parameters to the induced residual stresses. *Engineering Failure Analysis*, 15(8), 1097–1110. <https://doi.org/10.1016/j.engfailanal.2007.11.017>
- [20] Bagherifard, S., Ghelichi, R., & Guagliano, M. (2012a). Numerical and experimental analysis of surface roughness generated by shot peening. *Applied Surface Science*, 258(18), 6831–6840. <https://doi.org/10.1016/j.apsusc.2012.03.111>
- [21] Xu, Q., Cao, Y., Cai, J., Yu, J., & Si, C. (2021). The influence of ultrasonic shot peening on the surface roughness, microstructure, and mechanical properties of TC2 thin-sheet. *Journal of Materials Research and Technology*, 15, 384–393. <https://doi.org/10.1016/j.jmrt.2021.08.029>
- [22] Bagherifard, S., Ghelichi, R., & Guagliano, M. (2012b). On the shot peening surface coverage and its assessment by means of finite element simulation: A critical review and some original developments. *Applied Surface Science*, 259, 186–194. <https://doi.org/10.1016/j.apsusc.2012.07.017>
- [23] Song, C., Yang, C., Hu, S., & Yin, F. (2023). Numerical modeling of ultrasonic shot peening with an accurate impact velocity. *Journal of Manufacturing Processes*, 101, 982–989. <https://doi.org/10.1016/j.jmapro.2023.06.049>
- [24] Dwivedi, P. K., Sivateja, C., Rai, A. K., Ganesh, P., Basu, A., & Dutta, K. (2023). A comparative assessment of the effects of laser shock peening and ultrasonic shot peening on surface integrity and ratcheting fatigue performance of HSLA steel. *International Journal of Fatigue*, 176. <https://doi.org/10.1016/j.ijfatigue.2023.107902>

- [25] Wang, X., Xu, C., Hu, D., Li, C., Liu, C., & Tang, Z. (2021). Effect of ultrasonic shot peening on surface integrity and fatigue performance of single-crystal superalloy. *Journal of Materials Processing Technology*, 296. <https://doi.org/10.1016/j.jmatprotec.2021.117209>
- [26] Xu, C., Wang, X., Geng, Y., Wang, Y., Sun, Z., Yu, B., Tang, Z., & Dai, S. (2023). Effect of shot peening on the surface integrity and fatigue property of gear steel 16Cr3NiWMoVNB at room temperature. *International Journal of Fatigue*, 172. <https://doi.org/10.1016/j.ijfatigue.2023.107668>
- [27] Badreddine, J., Rouhaud, E., Micoulaut, M., Reintant, D., Remy, S., François, M., Viot, P., Doubre-Baboeuf, G., Le Saunier, D., & Desfontaine, V. (2011). Simulation and experimental approach for shot velocity evaluation in ultrasonic shot peening. *Mecanique et Industries*, 12(3), 223–229. <https://doi.org/10.1051/meca/2011114>
- [28] Zhao, G., Tian, Y., Li, H., Ma, L., Li, Y., & Li, J. (2024). Microstructure evolution and dynamic recrystallization mechanisms of 316L stainless steel during hot deformation. *Archives of Civil and Mechanical Engineering*, 24(1). <https://doi.org/10.1007/s43452-023-00844-y>
- [29] Philip, A. M., & Chakraborty, K. (2023). The Johnson Cook model for the machinability study. *Materials Today: Proceedings*, 80, 357–362. <https://doi.org/10.1016/j.matpr.2023.02.371>
- [30] Mahalle, G., Kotkunde, N., Kumar Gupta, A., & Singh, S. K. (2019). Cowper-Symonds Strain Hardening Model For Flow Behaviour Of Inconel 718 Alloy. In *Materials Today: Proceedings* (Vol. 18). [www.sciencedirect.comwww.materialstoday.com/proceedings2214-7853](http://www.sciencedirect.comwww.materialstoday.com/proceedings2214-7853)
- [31] Gao, S., Yu, X., Li, Q., Sun, Y., Hao, Z., & Gu, D. (2024). Research on dynamic deformation behavior and constitutive relationship of hot forming high strength steel. *Journal of Materials Research and Technology*, 28, 1694–1712. <https://doi.org/10.1016/j.jmrt.2023.12.096>

- [32] Li, H., Li, F. hui, Zhang, R., & Zhi, X. dong. (2023). High strain rate experiments and constitutive model for Q390D steel. *Journal of Constructional Steel Research*, 206. <https://doi.org/10.1016/j.jcsr.2023.107933>
- [33] Aberbache, H., Mathieu, A., Bolot, R., Bleurvacq, L., Corolleur, A., & Laurent, F. (2024). Experimental analysis and numerical simulation of Laser welding of thin austenitic stainless-steel sheets using two models: Bilinear isotropic strain hardening model and Johnson–Cook model. *Journal of Advanced Joining Processes*, 9. <https://doi.org/10.1016/j.jajp.2024.100198>
- [34] Ebrahimi, A., & Hermans, M. J. M. (2023). Laser butt welding of thin stainless steel 316L sheets in asymmetric configurations: A numerical study; Laser butt welding of thin metal sheets. *Journal of Advanced Joining Processes*, 8. <https://doi.org/10.1016/j.jajp.2023.100154>
- [35] Rahman Chukkan, J., Vasudevan, M., Muthukumaran, S., Ravi Kumar, R., & Chandrasekhar, N. (2015). Simulation of laser butt welding of AISI 316L stainless steel sheet using various heat sources and experimental validation. *Journal of Materials Processing Technology*, 219, 48–59. <https://doi.org/10.1016/j.jmatprotec.2014.12.008>
- [36] Ning, J., & Liang, S. Y. (2018). Model-driven determination of Johnson-Cook material constants using temperature and force measurements. *International Journal of Advanced Manufacturing Technology*, 97(1–4), 1053–1060. <https://doi.org/10.1007/s00170-018-2022-x>
- [37] Sanjurjo, P., Rodríguez, C., Peñuelas, I., García, T. E., & Belzunce, F. J. (2014). Influence of the target material constitutive model on the numerical simulation of a shot peening process. *Surface and Coatings Technology*, 258, 822–831. <https://doi.org/10.1016/j.surfcoat.2014.07.075>
- [38] Bagherifard, S., Ghelichi, R., & Guagliano, M. (2010). A numerical model of severe shot peening (SSP) to predict the generation of a nanostructured surface layer of material. *Surface and Coatings Technology*, 204(24), 4081–4090. <https://doi.org/10.1016/j.surfcoat.2010.05.035>

- [39] Chen, J. S., Desai, D. A., Heyns, S. P., & Pietra, F. (2019). Literature review of numerical simulation and optimisation of the shot peening process. In *Advances in Mechanical Engineering* (Vol. 11, Issue 3). SAGE Publications Inc. <https://doi.org/10.1177/1687814018818277>
- [40] Yin, F., Hu, S., Hua, L., Wang, X., Suslov, S., & Han, Q. (2015). Surface Nanocrystallization and Numerical Modeling of Low Carbon Steel by Means of Ultrasonic Shot Peening. *Metallurgical and Materials Transactions A: Physical Metallurgy and Materials Science*, 46(3), 1253–1261. <https://doi.org/10.1007/s11661-014-2689-z>
- [41] Miao, H. Y., Perron, C., & Lévesque, M. (n.d.). *FINITE ELEMENT SIMULATION OF SHOT PEENING AND STRESS PEEN FORMING*.
- [42] Tamer, Y., Toros, S., & Ozturk, F. (2023). Numerical and Experimental Comparison of Fractural Characteristics of 316L Stainless Steel. *Journal of Materials Engineering and Performance*, 32(3), 1103–1118. <https://doi.org/10.1007/s11665-022-07152-1>
- [43] Wang, C., Guo, Z., Zhou, B., Li, B., Fei, S., Deng, H., & Shen, G. (2024). Experimental investigation and numerical study on evolution of surface roughness caused by ultrasonic shot peening of 2024 aluminum alloy sheet. *Journal of Materials Research and Technology*, 30, 9061–9083. <https://doi.org/10.1016/j.jmrt.2024.05.254>
- [44] Al. (n.d.). *Données techniques des billes céramiques et autres matières dures Caractéris)ques Céramique*.
- [45] Dell'informazione. (n.d.). *SCUOLA DI INGEGNERIA INDUSTRIALE E Numerical Modelling of Soft Blasting on Polymeric Materials and Validation With Experimental Activities*.

# Appendix

Table A.1 Abbreviations

Abbreviation	Full name
USP	Ultrasonic shot peening
FEA	Finite Element Analysis
HAZ	Heat Affected Zone
CSP	Conventional Shot Peening
COR	Coefficient of Restitution
wrt	With respect to